



**HAL**  
open science

# Lateral structure variations and transient swarm revealed by seismicity along the Main Himalayan Thrust north of Kathmandu

R. Hoste-Colomer, L. Bollinger, H Lyon-Caen, A. Burtin, L. Adhikari

► **To cite this version:**

R. Hoste-Colomer, L. Bollinger, H Lyon-Caen, A. Burtin, L. Adhikari. Lateral structure variations and transient swarm revealed by seismicity along the Main Himalayan Thrust north of Kathmandu. *Tectonophysics*, 2017, 714-715, pp.107-116. 10.1016/j.tecto.2016.10.004 . hal-01992579

**HAL Id: hal-01992579**

**<https://hal.science/hal-01992579>**

Submitted on 24 Oct 2019

**HAL** is a multi-disciplinary open access archive for the deposit and dissemination of scientific research documents, whether they are published or not. The documents may come from teaching and research institutions in France or abroad, or from public or private research centers.

L'archive ouverte pluridisciplinaire **HAL**, est destinée au dépôt et à la diffusion de documents scientifiques de niveau recherche, publiés ou non, émanant des établissements d'enseignement et de recherche français ou étrangers, des laboratoires publics ou privés.

1 **Title: Lateral structure variations and transient swarm revealed by seismicity along the**  
2 **Main Himalayan Thrust North of Kathmandu**

3 **Authors:** R. Hoste-Colomer<sup>(1)(2)</sup>, L. Bollinger<sup>(1)</sup>, H. Lyon-Caen<sup>(2)</sup>, A. Burtin<sup>(3)</sup>, L.B. Adhikari<sup>(4)</sup>

4 <sup>(1)</sup> CEA, DAM, DIF, F-91297 Arpajon, France.

5 <sup>(2)</sup> Laboratoire de Géologie, Ecole Normale Supérieure/CNRS UMR 8538, PSL Research  
6 University, Paris 75005, France.

7 <sup>(3)</sup> Institut de Physique du Globe de Paris, Sorbonne Paris Cité, Université Paris Diderot,  
8 UMR 7154 CNRS, Paris, France.

9 <sup>(4)</sup> Department of Mines and Geology, National Seismological Center, Kathmandu,  
10 Nepal.

11 **Corresponding Author:** Roser Hoste-Colomer

12 Phone: +33 1 69 26 54 63

13 e-mail: [roser.hoste-colomer@cea.fr](mailto:roser.hoste-colomer@cea.fr)

14 **ABSTRACT**

15 The midcrustal seismicity along the Main Himalayan Thrust in Nepal presents lateral  
16 variations along the rupture of the 2015 Gorkha earthquake. In order to resolve these  
17 variations, we relocate the seismicity north of Kathmandu, during a period well covered by  
18 the Nepal National Seismological Network, using a double-difference algorithm. The 550  
19 relocated events highlight a complex pattern of clustered seismicity within the unstable-  
20 stable transition zone. Part of the seismicity is densely clustered on a southward dipping  
21 plane which ruptured on January 31<sup>st</sup> 1997 (ML=5.8), activating a backthrust with a  
22 geometry consistent with the centroid moment tensor of this event calculated in this study.

23 At its eastern end, the midcrustal cluster is offset by 20 km to the south suggesting the  
24 presence of a tear fault. The analysis of the time sequence allows constraining a scenario  
25 involving stress transfer between these local midcrustal structures, beginning more than one  
26 month before the 1997 main shock. The temporal evolution of the seismicity is strikingly  
27 similar for two other transient seismic swarm episodes which developed hundreds of  
28 kilometers apart along the Main Himalayan Thrust at the same time. The local stress field  
29 appears responsible for the higher sensitivity of these regions to subtle strain transients  
30 developing along the Main Himalayan Thrust.

31 **Key words:** seismicity, Main Himalayan Thrust, fault segmentation, relative relocation.

32

33

34

35

36

37

38

39

40

41

42

43

44

45 **1. Introduction**

46 Along-strike variations of seismic activity on a fault can result from lateral variations in the  
47 geometry of the locked fault zone, spatial heterogeneity in frictional parameters or from  
48 unsteady loading during the interseismic period. Variations in seismicity rates along the  
49 downdip end of a locked megathrust may reveal that the structure is segmented, and these  
50 segment boundaries may correspond to the barriers that delimit major seismic ruptures (e.g.  
51 Schwartz et al., 1989; Collot et al., 2004; Métois et al., 2012; Holtkamp et al., 2011;  
52 Holtkamp and Brudzinski, 2011). The Main Himalayan Thrust (MHT) fault in Nepal qualifies  
53 as one interesting fault to document in terms of seismicity variations given its seismogenic  
54 potential and the possible control of the coseismic ruptures by persistent structural features  
55 (e.g. Grandin et al., 2015). Indeed, despite the apparent homogeneity of the stress build up  
56 revealed by geodesy (Ader et al., 2012; Stevens and Avouac, 2015) significant variations of  
57 the seismic rate have been reported along strike (Pandey et al., 1999). Some of the  
58 variations in seismic rate are persistent in time and might reveal lateral heterogeneity in  
59 terms of seismic coupling and/or tectonic structures along strike of the MHT. Others are  
60 temporary, related to transient episodes including swarm activity or mainshock-aftershock  
61 sequences.

62 On April 25 2015 at 11h56 Nepal Standard Time (06h11 UTC), the Mw 7.8 Gorkha  
63 earthquake ruptured a 120 km-long and 35-50 km wide fault segment of the MHT (e.g.,  
64 Avouac et al., 2015; Grandin et al., 2015; Kobayashi et al., 2015; Elliott et al., 2016)(Figure 1),  
65 abutting the great M8.2 1934 earthquake rupture. The propagation of the rupture and the  
66 slip along the fault plane were heterogeneous, leading some authors to suggest possible

67 along strike variations of the structure at depth (Grandin et al., 2015, Fan and Shearer,  
68 2015).

69 The aftershocks near the trace of the rupture in the vicinity of Kathmandu are  
70 heterogeneously distributed (Adhikari et al., 2015; Bai et al., 2015). Some aftershocks are  
71 clustered under Kathmandu valley, a place where no seismicity has been observed during  
72 the interseismic period (Figure 1). In the meantime, north of the Nepalese capital, the  
73 aftershocks epicenters coincide with the location of the midcrustal interseismic cluster (10-  
74 20 km depth) (Figure1). The heterogeneous distribution of the Gorkha earthquake  
75 aftershocks and the seismicity during interseismic period north of Kathmandu could be due  
76 to structural complexities or a transient event. The goal of our study is to use small  
77 earthquakes prior to the 2015 Gorkha event to resolve structural and frictional  
78 characteristics that might control the rupture parameters of the main shock.

79 In order to test such a hypothesis, we analyze the spatio-temporal variations of the  
80 seismicity during the interseismic period north of Kathmandu, a region well covered by the  
81 Nepalese national seismological network. We first relocate the seismic events using a  
82 double-difference algorithm (Waldhauser and Ellsworth, 2000) and perform a Centroid  
83 Moment Tensor inversion of the largest instrumentally recorded event in the region, ML=5.8  
84 on January 31<sup>st</sup> 1997. We then interpret the spatial pattern of seismicity in terms of  
85 geological structures at depth, and finally focus on the temporal variation of the seismicity  
86 rate along this structure.

## 87 **2. Data description**

### 88 **2.1. Regional Network**

89 The seismicity of central and eastern Nepal has been continuously monitored since the  
90 1990s by the National Seismological Centre of Nepal (NSC) with a national network  
91 composed of 21 short period vertical component seismic stations. Among them 12 high gain  
92 stations have been operational since 1994 in central and eastern Nepal providing a  
93 completeness of the seismic catalogue for that region around local magnitude  $ML=2.0$   
94 (Pandey et al., 1999). Their records are processed using Jade-Onyx acquisition-treatment  
95 software in which a 1D velocity model is used to locate earthquakes using the phases picked  
96 manually at NSC (Pandey, 1985; Pandey et al., 1995, Adhikari et al., 2015). A complementary  
97 network of 3 stations was deployed temporarily, from July 1995 to December 1996. The  
98 addition of these stations facilitated improved locations for the small earthquakes generated  
99 at midcrustal depths below the front of the high topography (Cattin and Avouac, 2000) in the  
100 vicinity of the Main Himalayan shear zone (Nabelek et al., 2009).

## 101 **2.2. Earthquake catalogue**

102 North of Kathmandu, the interseismic activity appears concentrated at midcrustal depths  
103 within a permanent seismic cluster (Pandey et al., 1995; Cattin and Avouac, 2000) (Figure 1)  
104 modulated by a few transient seismicity bursts (Figure 2). The most important seismicity  
105 burst was recorded in 1997. Indeed, 30% of the  $ML \geq 4.0$  events of the catalogue in this  
106 region occurred in that year (Figure 2). The sequence culminated after the occurrence of the  
107 “Sarshin earthquake” an  $ML=5.8$  event which happened on January 31<sup>st</sup> 1997 (Table 1), an  
108 event preceded 3 hours before by a foreshock of  $ML 5.1$ . This event resulted in a maximum  
109 shaking intensity of  $MMI VII$  and was felt in Kathmandu 40 km SE from its epicenter. It  
110 caused significant impact ( $MMI VI$ ) over a region  $1800 \text{ km}^2$  in size (Sapkota, 2011). Given its  
111 magnitude, this event was also recorded at teleseismic distances by international

112 institutions, which assigned a body-wave magnitude (mb) around 5.2 and depths between  
113 17 and 23 Km (Table 1).

114 The Sarshin earthquake was followed by more than 160 aftershocks in a region spanning 50  
115 x 30 km<sup>2</sup>, a surface significantly larger than the expected rupture extension. The orientation  
116 of the seismic cluster based on NSC locations is unclear and we expect that relocated  
117 aftershocks will help to constrain the geometry of the structure activated by the Sarshin  
118 earthquake.

### 119 **3. Method**

#### 120 **3.1. Centroid Moment Tensor at regional scale**

121 Seismic data of the 1997 Sarshin earthquake recorded by stations at distances up to 1700 km  
122 and of good quality are used to calculate a Centroid Moment Tensor. This includes data from  
123 stations LSA (Tibetan plateau), HYB (central India), WUS (northern China) and CHTO  
124 (Thailand) (Figure 3).

125 The centroid moment tensor solution is retrieved from the inversion of regional long-period  
126 seismic waves (40-100s). The procedure is taken from Nábelek (1984) and is adapted to a  
127 low-frequency inversion (Nábelek and Xia, 1995). For the centroid moment tensor inversion,  
128 a 1-D velocity structure should be chosen to compute synthetic Green's functions and model  
129 the observed waveforms at seismic stations. Processing a large number of events (29  
130 earthquakes in (Burtin, 2005) and 107 earthquakes in (Baur, 2007) in the Himalaya and  
131 Tibetan Plateau regions) we failed to correctly invert the seismic waveforms at stations with  
132 a single velocity model. Seismic signals from sources occurring along the Himalayan arc were  
133 recorded at stations located around the Tibetan plateau and the India plate. Therefore,  
134 velocity structures through which seismic waves travel can drastically change. For instance

135 when a velocity model with a Moho depth fixed at 35 km (ex. India path) is used, the  
136 modeled waveforms for northern Tibetan stations will systematically arrive sooner than the  
137 observed ones. To overcome this issue, each ray path is associated with a specific 1-D  
138 structure. For the Indian station HYB, the model is from Saul et al., (2000) with a Moho  
139 depth at 35 km. For the Tibetan station LSA and northern China station WUS, the model is  
140 modified from Haines et al., (2003) with a Moho depth at 65 km. In this latter model, we had  
141 to remove the 5 km thick sedimentary layer because otherwise the synthetic inverted  
142 seismic waves were delayed too much. Finally, the model for the Thai station CHTO was set  
143 to an intermediate model between the Indian and Tibetan models with a Moho depth at 45  
144 km. These velocity models were tested using a trial and error procedure on the 29 focal  
145 mechanisms studied (Burtin, 2005); we retained those models that resulted in synthetics  
146 that best matched the observed seismic data (Figure 3) – See Burtin, 2005 for further  
147 information. Furthermore, for each earthquake analyzed in Burtin (2005), including the  
148 Sarshin earthquake, the centroid moment tensor source depth was constrained through a  
149 grid search algorithm that minimized the waveform misfit, using at first a coarse step size (10  
150 km) followed by a finer step size (1 km).

### 151 **3.2. Relative relocation at local scale**

152 We calculate relocations using the double-difference algorithm HypoDD (Waldhauser and  
153 Ellsworth, 2000) for the seismicity clustered north of Kathmandu, in the trace of the Gorkha  
154 earthquake. We use data from the NSC bulletin for the period 1996-1999 and the whole  
155 bulletin from the temporary experiment of 1995-1996. Relative locations are resolved by  
156 solving an inverse problem using a damped least-square technique, minimizing the residuals  
157 between observed and calculated phase delay times between a pair of adjacent earthquakes

158 recorded at common stations. This procedure reduces the biases induced by velocity model  
159 errors along the paths from hypocenters to seismic stations. The velocity model considered  
160 hereafter is the 1-D model of Pandey (1985) with a  $V_p/V_s$  of 1.73. We initially attribute to  
161 each seismic event the origin time and hypocenter of the NSC seismic bulletin. We also  
162 allocate location errors corresponding to the average of the longitudinal and latitudinal  
163 uncertainties as well as depth uncertainties documented in the bulletin. Undetermined  
164 depths in the database are fixed to 0. The second set of inputs include the arrival times of P  
165 and S phase arriving at a station for a given event. The weight for the P phases is fixed to 1  
166 and for the S phases to 0.3.

167 Given the very high density of events located immediately in the vicinity of the Sarshin  
168 earthquake, compared to the more diffuse spatial and temporal pattern of the seismicity  
169 elsewhere, we divide the catalogue of events in two, a western and an eastern region  
170 (respectively zones 1 and 2 hereafter) separated at 85.4E (Figure S1 and S3). This division will  
171 enable us to better optimize the relocation process.

172 We select pairs of phases at every station considering (1) a maximal separation between  
173 hypocenters of 20 km and (2) a minimum number of links between two neighbor events of 8  
174 for Zone 1 and of 4 for Zone 2.

175 The relocation is performed in both cases with P and S phases when available and with three  
176 sets of iterations taking into account the seismic bulletin parameters. We set the damping at  
177 20 in a LSQR inversion. The first set iterates four times using only P waves. The second set  
178 iterates also four times with P and S waves. The third set iterates 8 times taking into account  
179 P and S waves, limiting the residuals to 5 seconds and the maximum distance between linked  
180 pairs to 10 km. The relocation of Zone 1 considers 8 as the minimum number of links per pair

181 to form a continuous cluster. There is no clustering a priori parameter for the relocation of  
182 Zone 2.

183 We tested the most influential parameters for both the pair-phase selection and the  
184 relocation process. In the pair-phase selection, we tested values at 4, 8, and 12 for the  
185 minimum number of links between two neighbor events. We also tested maximum  
186 separation between hypocenters at 20 and 50 km. The number of pair-phases created  
187 increase considering either a larger number of minimum links per pair or a larger maximum  
188 separation distance between hypocenters, however there are more events weakly linked.  
189 The minimum number of links between two neighbor events tested changes in Zone 1 and 2  
190 because of the density of events. We also tested various numbers of iterations (4 and 8 for  
191 each set) in the relocation process. The RMS misfit decreases for the first two sets until it  
192 stabilizes after 4 iterations. The solution becomes unstable with 8 iterations, resulting in a  
193 centroid shift and in an unstable RMS misfit. In the third step, 8 iterations are needed to  
194 stabilize the RMS misfit. Geometrically, the relative relocations were similar for any iteration  
195 scheme.

196 The tests results support the parameters we chose for Zone 1 and 2.

#### 197 **4- Results**

198 In Zone 1 (Figure 4), the seismic bulletin includes 230 events with 2408 phases from which  
199 20140 P-phases pairs and 12469 S-phase pairs are found. 80% of P-phase pairs and 84% of S-  
200 phase pairs are selected. The event pairs have an average of 10 links with an average offset  
201 of 6.04 km. After event pair selection, 167 events are successfully relocated, with less than  
202 1500 m of 2-sigma-relative location errors in x, y, z and a RMS misfit reduction of 60%  
203 (Figure S2, S3, S5, and S6).

204 The seismic bulletin covering Zone 2 (Figure 4) includes 548 events with 4886 phases from  
205 which 45938 P-phase and 39002 S-phase pairs are determined. Respectively, 49% and 45%  
206 of P- and S-phase pairs are selected. The event pairs have an average of 6 links with an  
207 average offset of 6.9 km. 477 events are selected, from which 384 events are successfully  
208 relocated with less than 100 m of 2-sigma-relative location errors in x, y, z. The RMS misfit  
209 reduction, following the integration of the phases picked at the temporary 3 component  
210 stations, is close to 90% (Figure S2, S3, S4, S5, S6, and S7).

211 The relocation of Zone 1 and Zone 2 seismicity indicates the presence of two separate  
212 clusters during the 1997 seismic episode (Figure 4). The westernmost seismic cluster is  
213 located between  $85.3^\circ$  and  $85.4^\circ$ , covering an area of  $7 \times 11 \text{ km}^2$  (Figure 4, map), just above  
214 the January 31<sup>st</sup> Sarshin earthquake hypocenter (Figure 4, cross-section). The visual  
215 inspection of 3D plots shows that the seismicity lies on a plane that strikes  $N050 \pm 20 \text{ E}$   
216 dipping steeply southeast ( $70\text{-}80^\circ$ ). The other seismic cluster is smaller ( $6 \times 8 \text{ km}^2$ ) and is  
217 located between  $85.4^\circ$  and  $85.5^\circ$ . It describes an almost vertical plane striking  $N155 \pm 20 \text{ E}$   
218 (Figure 4). No large event is associated with this cluster. The remaining relocated seismic  
219 events do not show a particular geometry. Most of them are located in a 10 km-wide band  
220 east of  $85.5^\circ$ .

221 The centroid moment tensor solution for the January 31<sup>st</sup> Sarshin earthquake indicates a  
222 best centroid depth at 17 km and a reverse motion with a slight strike-slip component. One  
223 nodal plane (NP1) strikes  $N075$  and dips  $85^\circ \text{SE}$ , and the second (NP2) strikes  $N152$  and dips  
224  $24^\circ \text{NE}$ . Although it is difficult to quantify uncertainties on the centroid moment tensor  
225 solution, the azimuthal coverage being decent and the changes in centroid moment tensor  
226 being small in the vicinity of the best depth, we consider the uncertainties to be moderate

227 (+/-20°) (Zahradnik et al., 2008). In particular NP1, which dips at a high angle, is quite stable  
228 in the inversions. The NP1 plane is the closest to the plane defined by the relocated  
229 aftershocks of the Sarshin earthquake. The moment magnitude obtained is  $M_w=4.8$ .

230 The depths of the relocated events range from 15 to 26 km in the western cluster, with the  
231 main shock at 24 km depth which is slightly deeper than previous determinations (Table 1).  
232 NSC gives a hypocenter at 20.3 km while the centroid moment tensor centroid depth is at 17  
233 km. Although the relocation allows us to place constraints on the relative positions of  
234 hypocenters leading to a fairly well defined geometry for the cluster, the centroid depth of  
235 the cluster (~22 km) is less well constrained as the closest station that recorded these events  
236 is located at ~ 25 km, and thus the centroid could move by a few kilometers. Both  
237 hypocenter depths and centroid moment tensor centroid depths being within +/-5 km, we  
238 think the differences may not be significant. In addition, as most crustal earthquakes  
239 nucleate at depth and propagate towards the surface (e.g., Das and Scholz, 1983; Huc et al.,  
240 1998), we expect the hypocenter depth of the mainshock to be larger than its centroid  
241 moment tensor depth. This will be particularly true if the co-seismic slip is small and the  
242 ruptured area large for a  $M_w4.8$  event. Indeed, the source of a  $M_w4.8$  can be either  $2 \times 2 \text{ km}^2$   
243 with 10cm of slip or  $5 \times 5 \text{ km}^2$  with 2 cm of slip.

## 244 **5- Interpretation**

### 245 **Spatial distribution of the Sarshin Swarm**

246 Most of the 1996-2000 Sarshin Swarm seismicity is located at midcrustal depths, with  
247 centroid depths at 22 and 15 km respectively for the two clusters (Figure 4). These depths  
248 roughly correspond to the depth of the Main Himalayan shear zone, as interpreted on

249 images obtained along profiles based on receiver function analysis (Schulte-Pelkum et al.,  
250 2005; Nabelek et al., 2009; Duputel et al., 2016).

251 The westernmost cluster develops after the main shock of the Sarshin earthquake over a 7 x  
252 11 km<sup>2</sup> region. Given the geometry of the cluster and the fault plane solution parameters of  
253 its main shock, the January 31<sup>st</sup> 1997 Sarshin earthquake, we associate this seismic swarm to  
254 the activation of a NE-SW backthrust, steeply dipping to the southeast. Assuming that the  
255 aftershock distribution corresponds to the maximum extent of the fault segment ruptured  
256 by the main shock, a Mw 4.8 ( $M_0 = 2.3 \cdot 10^{16}$  Nm deduced from the centroid moment tensor  
257 determination), and assuming a shear modulus of 32 GPa we obtain an average minimum slip  
258 of 1 cm. Considering that aftershocks may more likely extend beyond the edges of the  
259 ruptured plane, its surface is likely overestimated. A surface overestimation by 100% will  
260 lead to doubling the average slip, at 2 cm. This amount of slip at depth induces infra-mm  
261 displacements at the surface GPS sites around, values below the resolution capacity of the  
262 campaign GPS available at that time (Jouanne et al., 2004).

263 A rupture on a steep south-eastward dipping - northwestward verging thrust at mid-crustal  
264 depths below the front of the high topography may correspond either to the activation of (a)  
265 a fault segment at the forelimb of the lesser Himalayan duplex (e.g. Pearson and DeCelles,  
266 2005; Khanal and Robinson, 2013), or (b) a local shear zone within the hinge above the flat-  
267 decollement/ramp, as predicted by mechanical models (Souloumiac et al., 2009) (Figure 7D).  
268 We prefer the latter interpretation, as the depth seems more consistent with the downdip  
269 end of a midcrustal ramp than the passive roof-thrust of the duplex.

270 The relocated seismicity appears offset by 20 km from west to east, describing an eastward  
271 right-stepping strand. Note that this step is not an artifact due to the location of the

272 boundary between the two zones considered in the relocation process: alternative  
273 relocations considering only one zone, keeping the same relocation parameters, produced  
274 similar spatial patterns, with the seismic cluster stepping to the south in this area. This offset  
275 could be explained by the presence of a tear fault between two ramps or structural  
276 discontinuities within the Main Himalayan shear zone such as a stepover of the fault. We  
277 prefer the former hypothesis given the absence of overlapping seismicity along strike. In  
278 addition, the vertical NW-SE plane described by the second cluster (85.4° and 85.5°)  
279 identified in the relocation results is consistent with tear faulting although we could not  
280 compute any fault plane solution to prove this. Such tear faults are required because of the  
281 topology of the MHT flat/ramp system and its lateral variations (Figure 7). The right lateral  
282 tear fault suspected to develop at depth within the trace of the second cluster is aligned  
283 with an active dextral fault system reaching the surface along the 20 km-long NNW-SSE Jhiku  
284 Kholā fault (Kumahara et al., 2016).

285 We propose that the backthrust and tear fault activated during the 1997 seismic episode,  
286 and in a more general way every significant variation of the structure at depth along the  
287 MHT, might influence its behavior. It could affect the propagation of the co-seismic rupture  
288 (e.g. Béjar-Pizarro et al., 2010), influencing the co- and post-seismic slip distribution as well  
289 as the location of the aftershocks. Note that the structure we studied is located in between  
290 two patches of maximum slip of the Gorkha earthquake proposed by some authors (e.g.  
291 Avouac et al., 2015; Grandin et al., 2015) (Figure 1).

## 292 **Temporal distribution of the seismicity at local and regional scales**

293 The time structure of a seismic **episode** gives a dynamic sense and evolution of the  
294 phenomenon that the spatial distribution does not. Both are essential to interpret our  
295 results.

296 The time structure of the seismicity in this area (Figure 4) exhibits complex variations in the  
297 period covered by our study. The seismicity rate decreases first in mid-1996 (Figure 2 and 5).  
298 This relative quiescence is difficult to ascertain, being concurrent with the monsoon arrival, a  
299 period during which the seismic noise level and therefore the completeness magnitude of  
300 the catalogue is higher than on average, a period during and slightly after which the seasonal  
301 load of the India plate has a genuine influence on the seismicity (Bollinger et al., 2007;  
302 Bettinelli et al., 2008; Burtin et al., 2008). The seismic rate remains low until December, far  
303 after the monsoon period, and is followed by a sharp increase. The seismic events are then  
304 clustered between  $85.4^\circ$  and  $85.5^\circ$  (Central zone in Figure 4), mostly along a 6 km-long  
305 vertical plane oriented N155. This activity, decreasing at the beginning of 1997, is followed  
306 by the development of another cluster 15 km to the northwest in January (Figure 4, 5). The  
307 swarm in the area begins before the Sarshin main shock which occurred at 20:02 (local time)  
308 on January 31st and was preceded by a ML5 and smaller events a few hours earlier. The  
309 seismic cluster that developed within the next three months within 10 km from the  
310 hypocenter is typical of an aftershock sequence. In the meantime, the seismicity rate east of  
311  $85.5^\circ\text{E}$  increased significantly (Figure 5).

312 Surprisingly, this unusual transient seismic activity is not exceptional in the Himalaya region.  
313 Indeed, in eastern Nepal, a seismic swarm developed between  $86.8$  and  $87^\circ\text{E}$ , generating 80  
314 events south of Mount Everest, between November 1996 and May 1997. No main shock was  
315 detected prior to the onset of the seismic swarm but a larger shock, with a ML 5.8, occurred  
316 on the 30/12/1996 (Table 1) and was followed by aftershocks (Figure 6). In western Nepal,

317 between 80.5° and 81°E, a similar swarm developed with a main shock on 05/01/1997 of  
318 ML=6.3 (Table 1). The location of the seismicity in these two areas is not sufficiently resolved  
319 to perform an analysis similar to what has been done here. The time structure of these two  
320 swarms is very similar to that of Sarshin as illustrated on Figure 6.

321 Altogether, the 3 clusters contribute to 40% of the yearly midcrustal events detected along  
322 the front of the range in Nepal. Their cumulative along strike development accounts for ~ 10  
323 % of the length of the midcrustal cluster making this event the most important seismicity  
324 burst of the interseismic period recorded by the Nepal National Seismological Network. No  
325 significant seismic rate variations were detected in between the three clusters (Figure 6).

## 326 **6- Discussion**

327 Complex spatial and temporal variations of seismicity have been revealed at local and  
328 regional scales. Locally, north of Kathmandu, the spatial distribution of the seismicity  
329 coincides with a back-thrust and a thrust segment separated by a proposed 20 km-long tear  
330 fault. Their consecutive activation follows the development of a seismic swarm on the tear  
331 fault. The geometry of the fault system is consistent with a right lateral slip on the tear fault.  
332 This scenario is compatible with the topology of the thrust system as well as with the  
333 kinematics of the dextral NNW-SSE Jhiku Khola fault described in continuity to the south  
334 (Kumahara et al., 2016). The en-echelon segments of the MHT there are close to the  
335 unstable-stable transition zone USTZ (e.g. Jackson and Bilham, 1994; Bettinelli et al., 2006).  
336 This behavior was confirmed recently by the determination of the seismic coupling that falls  
337 there between 0.4 and 0.6 (Ader et al., 2012; Grandin et al., 2012; Stevens and Avouac,  
338 2015).

339 The seismic activity in 1997 in this region could result from (1) a local unsteady loading or (2)  
340 a local strain transfer in the vicinity of the USTZ. However, rather than just a local strain

341 transient, the development in 1996-97 of 2 other clusters hundreds of kilometers apart,  
342 depicting similar temporal variations, may imply (3) a large scale unsteady loading. The  
343 unsteady loading could be due, among others, to a lithospheric response to the water mass  
344 redistribution after the monsoon or to a slow slip event. However, in 1996, the precipitation  
345 records were fairly typical (e.g., Shrestha et al., 2000; Yatagai et al., 2012). This leads us to  
346 propose that the 1997 seismic episode may be related to a slow slip event. A transient slip  
347 event with a slip amplitude of tens of centimeters is precluded due to the absence of  
348 measurable changes in the seismicity rate between the clusters (Figure 6A). Indeed, a  
349 seismicity change would likely occur after a centimetric to decimetric scale slow slip event,  
350 which would in turn release years of stress build up and therefore most probably induce  
351 years of midcrustal seismicity along strike. The lower end of the slip amplitude expected, i.e.  
352 1 cm, would correspond roughly to the seismic slip accommodated during the Sarshin  
353 earthquake (see previous section for estimation). In Sarshin area, such an amount of slip at  
354 midcrustal depths generates only infra-millimetric displacements at RAM0 and SYA0,  
355 regional GPS stations respectively 17 and 20 km from the updip-end of the ruptured fault  
356 plane. These stations were surveyed briefly in 1995 and 1998 (1 to 4 days/sessions). They  
357 were translated in 3 years by  $19\pm 6$  mm and  $21\pm 7$  mm respectively in an India fixed reference  
358 frame (Jouanne et al., 2004). The large uncertainties of the measurements preclude  
359 resolving the infra-millimetric displacements induced by the Sarshin earthquake as well as  
360 those induced by any strain transient with similar amplitudes. We further note that the  
361 displacements uncertainties for both stations amounts to one third of the measurements, a  
362 value comparable to one year of strain above the Main Himalayan Thrust. The thrust  
363 accommodates, at depth, on average, a shortening of 18 mm/yr (Ader et al., 2012).  
364 Detecting a transient slip event at depth on the creeping part of the MHT of less than 18 mm

365 therefore seems impossible. This result is corroborated by the absence of any major change  
366 in the shortening rates estimated elsewhere in Nepal by campaign GPS data, and by the  
367 continuous DORIS time series available at Everest.

368 Several of the large transient events elsewhere in the world were accompanied by tremors  
369 and low frequency earthquakes (Schwartz and Rokosky, 2007). Such kinds of seismic events  
370 have not been observed in 1997 in Nepal, a period during which the continuous seismic  
371 signals recorded by National Seismological Network was not stored. Further analysis of these  
372 signals to detect tremors or low frequency earthquakes is therefore limited to the cut signals  
373 of seismic events which, according to a preliminary analysis, present a typical spectra.

374 Despite the lack of direct evidence that tremors and low frequency earthquakes occurred,  
375 we think the seismic catalogue contains other indirect evidences of this process.

376 A subtle transient slip event may generate heterogeneous seismicity along strike due to the  
377 geometry and state of stress changes along strike of the MHT. Indeed, the midcrustal  
378 seismicity under the front of the Himalayas appears sensitive to the local state of stress  
379 which depends mainly on the regional tectonic stress and the topography, through their  
380 influence on the preferred orientation of the failure planes (Bollinger et al., 2004a). In  
381 between the Main Frontal Thrust and the front of the High range, S3 and S1, the minimal  
382 and maximal principal stresses, are respectively vertical and north-south. S1 increases during  
383 interseismic deformation due to slip at depth on the MHT, promoting failure on EW striking  
384 thrust planes (Figure 7A(area 2)). Further north, in the Southern Tibetan grabens (Figure 6B),  
385 S1 is vertical while S3 is horizontal, striking approximately east-west. S3 might decrease  
386 during interseismic deformation (Figure 7A(area 3)), since east-west extension increases in  
387 the Southern Tibetan Graben due to the divergence of thrusting along the Himalayan Arc  
388 (Bollinger et al., 2004a). This promotes failure on north-south oriented normal faults (ie: the

389 southern Tibetan grabens). In between these two domains (i.e. south of the range, Tibetan  
390 Plateau: between area 2 and 3 on Figure 7A) the regional state of stress might promote the  
391 existence of NW-SE and NE-SW strike slip faults. This is valid for a range of depths in the  
392 cluster which depends on both  $S_1$  and  $S_3$  and the local non compensated topography. In this  
393 area, the intermediate stress component is vertical, while the maximum and minimum  
394 principal stresses correspond respectively to the north-south and east-west stress values  
395 (Figure 7A(area 1)). The strike slip faults in this region are very sensitive to the simultaneous  
396 N-S and E-W stress variations (Figure 7A). The lack of strike slip Centroid Moment Tensor  
397 solutions for intermediate events ( $M > 5.5$ ) during the last decades along the Himalaya  
398 demonstrate that strike slip faulting is infrequent along strike, probably due to the  
399 restriction to a small depth range of the corresponding state of stress. Besides the presence  
400 of large scale active strike-slip faults affecting the lesser Himalayas (Nakata, 1989),  
401 interpreted as resulting from large scale strain partitioning (Nakata, 1989; Murphy et al.,  
402 2014) or from the presence and migration of lateral ramps (Bollinger et al., 2004b), few  
403 active strike-slip fault segments were described at the foot of the High range (Nakata, 1989).  
404 However, tear-faults are suspected at midcrustal depths because of the lateral variations of  
405 the midcrustal ramps along the strike of the Main Himalayan thrust (e.g. Robinson et al.,  
406 2001; Bollinger et al., 2004b; Grandin et al., 2012). Despite the publication of balanced cross  
407 sections immediately west of Sarshin area (e.g. Pearson and Decelles, 2005; Khanal and  
408 Robinson, 2013), the present-day positions of the midcrustal ramps in the vicinity of the  
409 seismic cluster studied here are still unresolved. Assuming the cluster represents the edge of  
410 the MHT locked segment (e.g. Cattin and Avouac, 2000; Bollinger et al., 2004; Ader et al.,  
411 2012, Grandin et al., 2015), a dextral NW-SE transform structure is required for the sake of  
412 geometrical continuity (Figure 4 and 5, Central zone in blue). Assuming that this swarm is

413 located on such a right lateral strike slip segment, its activity in December 1996 creates static  
414 stress changes at its extremities. It leads to the generation of 2 positive Coulomb stress  
415 variations ( $\Delta CFF$ ) lobes on its NW and SE sides (while NE and SW would see a negative  
416  $\Delta CFF$ ) (Figure S8 to S11 and Table S2). This static stress change scenario accounts for the  
417 generation of seismicity along the backthrust to the NW and the thrust to the SE as well as  
418 with the lack of microseismic activity along its NE and SW extremities (Figure 7B and 7C).  
419 Furthermore it is consistent with Sarshin focal mechanism depicting a NE-SW oriented fault  
420 plane solution (Figure 4).

421 Whether similar kinematics and mechanisms are involved in the generation of the Far  
422 western and eastern Nepal seismic swarms is unknown. Unfortunately, the seismicity in  
423 these regions cannot be analyzed with a similar relocation approach due to the less optimal  
424 geometry of the seismic network and completeness of the database. But the 3 swarms are  
425 located in similar settings, within the midcrustal cluster at similar distances from the USTZ  
426 and within the trace of southern Tibetan Grabens (Figure 6B). Another similarity is their time  
427 sequence that begins with a weak but detectable decrease of seismicity prior to the swarms'  
428 development (Figure 6A). These rate decreases begin about 6 months prior to each swarm,  
429 during the onset of the monsoon. That the higher level of seismic noise during the monsoon  
430 is responsible for the seismic rate decrease is possible (Bollinger et al., 2007), but the rate  
431 remains low after the end of the monsoon and the decrease of the seismic noise generated  
432 by landsliding and rivers (Burtin et al., 2008). An alternative interpretation could be that the  
433 seismicity was partially inhibited and then promoted due to the response of the crust to a  
434 loading/unloading of continental water (Bettinelli et al., 2008; Chanard et al., 2014) in 1996.  
435 Whatever the scenario, the simultaneous development of these swarms may have resulted  
436 from a transient slip event similar to those detected along other subduction zones (e.g.

437 Cascadia, Mexico, Japan,...) with an affected area between 30 to 600 km along strike, and  
438 transient slip lasting 6 days to about a year with amplitudes between 5 mm and 5.6 cm (e.g.  
439 Dragert et al., 2001; Schmidt and Gao, 2010; Schwartz and Rokosky, 2007; Szeliga et al.,  
440 2008).

441 Such a slow slip event occurring on the Main Himalayan Thrust could play a role in the  
442 seismic cycle of the locked segment of the fault. Indeed, such transient events bring the  
443 locked fault zone closer to failure by several months (Dragert et al., 2001), besides the  
444 interseismic loading on the fault.

#### 445 **7- Conclusion**

446 The first conclusion to be drawn from this work is that the downdip end of the locked  
447 section of the Main Himalayan Thrust exhibits lateral seismicity variations that may reveal  
448 the presence of structural complexities at midcrustal depths. The right-stepping geometry of  
449 the seismicity, north of Kathmandu, is interpreted as resulting from the activation of a tear  
450 fault between a backthrust and a thrust segment. This structural complexity might have  
451 influenced the slip distribution during the Gorkha earthquake rupture as revealed by a local  
452 minima in the region of high slip of some published slip models. A second major conclusion  
453 is that the time sequence of the seismic swarm which developed there in 1996-97 is  
454 consistent with a propagation of a local strain transient, from the tear fault to the backthrust  
455 and thrust. Finally, the temporal coincidence between this swarm and two others at far  
456 distances leads us to suspect the development of a larger-scale transient slip event on the  
457 Main Himalayan Thrust. The local stress field appears responsible for the higher sensitivity of  
458 these areas to strain transients and needs therefore to be monitored to ascertain the  
459 presence of infrequent subtle slow slip events along the Himalaya.

#### 460 **Acknowledgements**

461 This project is funded by the French Agence Nationale de la Recherche (ANR-13-BS06-0006-  
462 01) and the Commissariat à l’Energie Atomique et aux Energies Alternatives. We thank the  
463 National Seismological Centre, Sudhir Rajaure and Soma Nath Sapkota for early exchanges  
464 on the seismic catalogue and macroseismic field of the Sarshin earthquake. The authors also  
465 thank the two anonymous reviewers and Gavin P. Hayes for their helpful comments that  
466 improved the paper.

## 467 **References**

468 Ader, T., Avouac, J.P., Liu-Zeng, J., Lyon-Caen, H., Bollinger, L., Galetzka, J., Genrich, J.,  
469 Thomas, M., Chanard, K., Sapkota, S.N., Rajaure, S., Shrestha, P., Ding L. and Flouzat, M.,  
470 2012. Convergence rate across the Nepal Himalaya and interseismic coupling on the Main  
471 Himalayan Thrust: Implications for seismic hazard, *Journal of Geophysical Research*, 117,  
472 B04403, doi: 10.1029/2011JB009071.

473 Adhikari, L.B., Gautam, U.P., Koirala, B.P., Bhattarai, M., Kandel, T., Gupta, R.M., Timsina, C.,  
474 Maharjan, N., Maharjan, K., Dahal, T., Hoste-Colomer, R., Cano, Y., Dandine, M., Guilhem, A.,  
475 Merrer, S., Roudil, P. and Bollinger, L., 2015. The aftershock sequence of the 2015 April 25  
476 Gorkha-Nepal earthquake, *Geophysical Journal International*, 203, 2119-2124, doi:  
477 10.1093/gji/ggv412.

478 Armijo, R., Tapponnier, P., Mercier, J.L. and Han, T.L., 1986. Quaternary extension in southern  
479 Tibet: Field observations and tectonic implications, *Journal of Geophysical Research: Solid*  
480 *Earth*, 91 (B14), 13803-13872.

481 Avouac, J.P., Meng, L., Wei, S., Wang, T. and Ampuero, J.P., 2015. Lower edge of locked Main  
482 Himalayan Thrust unzipped by the 2015 Gorkha earthquake, *Nature Geoscience*, 8, 708-711.

483 Bai, L., Liu, H., Ritsema, J., Mori, J., Zhang, T., Ishikawa, Y. and Li, G., 2015. Faulting structures  
484 above the Main Himalayan Thrust as shown by relocated aftershocks of the 2015 Mw7.8  
485 Gorkha, Nepal, earthquake, *Geophysical Research Letters*, 43, doi:10.1002/2015GL066473.

486 Baur, 2007. *Seismotectonics of the Himalayas and the Tibetan Plateau: Moment Tensor*  
487 *Analysis of Regional Seismograms*, Oregon State University, p.298.

488 Bettinelli, P., Avouac, J.P., Flouzat, M., Jouanne, F., Bollinger, L., Willis, P. and Chitrakar, G.R.,  
489 2006. Plate motion of India and interseismic strain in Nepal Himalaya from GPS and DORIS  
490 measurements, *Journal of Geodesy*, 80, 567-589, doi:10.1007/s00190-006-0030-3.

491 Bettinelli, P., Avouac, J.P., Flouzat, M., Bollinger, L., Ramillien G., Rajaure S. and Sapkota S.,  
492 2008. Seasonal variations of seismicity and geodetic strain in the Himalaya induced by  
493 surface hydrology, *Earth and Planetary Science Letters*, 266, 332-344,  
494 doi:10.1016/j.epsl.2007.11.02110.

495 Béjar-Pizarro, M., Carrizo, D., Socquet, A., Armijo, R., Barrientos, S., Bondoux, F., Bonvalot,  
496 S., Campos, J., Comte, D., de Chabalier, J.B., Charade, O., Delorme, A., Gabalda, G., Galetzka,  
497 J., Genricj, J., Nercessian, A., Olcay, M., Ortega, F., Ortega, I., Remy, O., Ruegg, J.C., Simons,  
498 M., Valderas, C. and Vigny, C., 2010. Asperities and barriers on the seismogenic zone in  
499 North Chile: state-of-the-art after the 2007 Mw 7.7 Tocopilla earthquake inferred by GPS  
500 and InSAR data, *Geophysical Journal International*, 183, 390-406, doi: 10.1111/j.1365-  
501 246X.2010.04748.x.

502 Bollinger, L., Avouac, J.P., Cattin, R. and Pandey, M.R., 2004a. Stress buildup in the Himalaya,  
503 *Journal of Geophysical Research*, 109, B11405, doi:10.1029/2003JB002911.

504 Bollinger, L., Avouac, J.P., Beyssac, O., Catlos, E.J., Harrison, T.M., Grove, M., Goffé, B. and  
505 Sapkota, S., 2004b. Thermal structure and exhumation history of the Lesser Himalaya in  
506 central Nepal, *Tectonics*, 23, TC5015, doi:10.1029/2003TC001564.

507 Bollinger, L., Perrier, F., Avouac, J.P., Sapkota, S., Gautam, U, and Tiwari, D.R., 2007.  
508 Seasonal modulation of seismicity in the Himalaya of Nepal, *Geophysical Research Letters*,  
509 34, L08304, doi:10.1029/2006GL029192.

510 Bollinger, L., Tapponnier, P., Sapkota, S.N. and Klinger, Y., 2016. Slip deficit in central Nepal:  
511 omen for a repeat of the 1344 AD earthquake?, *Earth, Planets and Space*, 68:12,  
512 doi:10.1186/s40623-016-0389-1.

513 Burtin, A., 2005. Seismotectonics of the Himalayan Arc from Regional Seismogram Moment  
514 Tensor Inversion, Internship report, Oregon State University.

515 Burtin, A., Bollinger, L., Vergne, J., Cattin R. and Nábělek J. L., 2008. Spectral analysis of  
516 seismic noise induced by rivers: A new tool to monitor spatiotemporal changes in stream  
517 hydrodynamics, *Journal of Geophysical Research*, 113, B05301, doi:10.1029/2007JB005034.

518 Cattin, R. and Avouac, J.P., 2000. Modeling mountain building and seismic cycle in the  
519 Himalaya of Nepal, *Journal of Geophysical Research*, 105(B6), 13389-13407.

520 Chanard, K., Avouac, J. P., Ramillien G. and Genrich J., 2014. Modeling deformation induced  
521 by seasonal variations of continental water in the Himalaya region: Sensitivity to Earth elastic  
522 structure, *Journal of Geophysical Research: Solid Earth*, 119, doi:10.1002/2013JB010451.

523 Collot, J. Y., Marcaillou, B., Sage, F., Michaud, F., Agudelo, W., Charvis, P., Graindorge, D.,  
524 Gutscher, M-A. and Spence, G., 2004. Are rupture zone limits of great subduction  
525 earthquakes controlled by upper plate structures? Evidence from multichannel seismic

526 reflection data acquired across the northern Ecuador–southwest Colombia margin, *Journal*  
527 *of Geophysical Research: Solid Earth*, 109, B11103.

528 Das, S. and Scholz, C.H., 1983. Why large earthquakes do not nucleate at shallow depths,  
529 *Nature*, 305, pp.621-623.

530 Dragert, H., Wang, K. and James, T. S., 2001. A silent slip event on the deeper Cascadia  
531 subduction interface, *Science*, 292(5521), 1525-1528.

532 Duputel, Z., Vergne, J., Rivera, L., Wittlinger, G., Farra, V. and Hetényi, G., 2016. The 2015  
533 Gorkha earthquake: A large event illuminating the Main Himalayan Thrust fault, *Geophysical*  
534 *Research Letters*, 43, doi: 10.1002/2016GL068083.

535 Elliott, J.R., Jolivet, R., Gonzalez, P.J., Avouac, J.P., Hollingsworth, J., Searle, M.P. and  
536 Stevens, V.L., 2016. Himalayan megathrust geometry and relation to topography revealed by  
537 Gorkha earthquake, *Nature geoscience*, 9, doi:10.1038/NGEO2623.

538 Fan, W. and Shearer P.M., 2015. Detailed rupture imaging of the 25 April 2015 Nepal  
539 earthquake using teleseismic P waves, *Geophysical Research Letters*, 42, 5744-5752, doi:  
540 10.1002/2015GL064587.

541 Grandin, R., Doin, M-P., Bollinger, L., Pinel-Puysegur, B., Ducret, G., Jolivet, R. and Sapkota,  
542 S.N., 2012. Long-term growth of the Himalaya inferred from interseismic InSAR  
543 measurement, *Geology*, 40, 12, 1059-1062, doi:10.1130/G33154.1.

544 Grandin, R., Vallée, M., Satriano, C., Lacassin, R., Klinger, Y., Simoes, M., and Bollinger, L.,  
545 2015. Rupture process of the Mw=7.9 2015 Gorkha earthquake (Nepal): insights into  
546 Himalayan megathrust segmentation, *Geophysical Research Letters*, 42, doi:  
547 10.1002/2015GL066044.

548 Haines, S.S., Klemperer, S.L., Brown, L., Jingru, G., Mechie, J., Meissner, R., Ross, A. and  
549 Wenjin, Z., 2003. INDEPTH III seismic data: From surface observations to deep crustal  
550 processes in Tibet, *Tectonics*, 22(8), 1001.

551 Huc, M., Hassani, R., and Chéry, J., 1998. Large earthquake nucleation associated with stress  
552 exchange between middle and upper crust, *Geophysical Research Letters*, 25 (4), 551-554.

553 Holtkamp, S. G. and Brudzinski, M. R., 2011. Earthquake swarms in circum-Pacific subduction  
554 zones, *Earth and Planetary Science Letters*, 305(1), 215-225.

555 Holtkamp, S. G., Pritchard, M. E. and Lohman, R. B., 2011. Earthquake swarms in south  
556 America, *Geophysical Journal International*, 187(1), 128-146.

557 Jackson, M., and Bilham, R., 1994. Constraints on Himalayan deformation inferred from  
558 vertical velocity fields in Nepal and Tibet, *Journal of Geophysical Research: Solid Earth*,  
559 99(B7), 13897-13912.

560 Jouanne, F., Mugnier, J.L., Gamond, J.F., Le Fort, P., Pandey, M.R., Bollinger, L., Flouzat, M.  
561 and Avouac, J.P., 2004. Current shortening across the Himalayas of Nepal, *Geophysical*  
562 *Journal International*, 157, 1-14, doi: 10.1111/j.1365-246X.2004.02180.x.

563 Khanal, S. and Robinson, D.M., 2013. Upper crustal shortening and forward modeling of the  
564 Himalayan thrust belt along the Budhi-Gandaki River, central Nepal, *International Journal of*  
565 *Earth Science (Geol Rundsch)*, 102, 1871-1891.

566 Kobayashi, T., Morishita, Y. and Yarai, H., 2015. Detailed crustal deformation and fault  
567 rupture of the 2015 Gorkha earthquake, Nepal, revealed from ScanSAR-based  
568 interferograms of ALOS-2, *Earth, Planets and Space*, 67, 201, doi: 10.1186/s40623-015-0359-  
569 z.

570 Kumahara, Y., Chamlagain, D., Upreti, B. N., 2016. Geomorphic features of active faults  
571 around the Kathmandu Valley, Nepal, and no evidence of surface rupture associated with  
572 the 2015 Gorkha earthquake along the faults, *Earth, Planets and Space*, 68(1), 1-8.

573 Métois, M., Socquet, A. and Vigny, C., 2012. Interseismic coupling, segmentation and  
574 mechanical behavior of the central Chile subduction zone, *Journal of Geophysical Research*,  
575 117, B03406, doi:10.1029/2011JB00736.

576 Murphy, M. A., Taylor, M. H., Gosse, J., Silver, C. R. P., Whipp, D. M. and Beaumont, C., 2014.  
577 Limit of strain partitioning in the Himalaya marked by large earthquakes in western Nepal,  
578 *Nature Geoscience*, 7(1), 38-42.

579 Nábelek, J., 1984. Determination of earthquake source parameters from inversion of body  
580 waves. Ph. D. thesis, Massachusetts Institute of Technology, Cambridge, MA.

581 Nábelek, J. and Xia, G., 1995. Moment-tensor analysis using regional data: Application to the  
582 25 March, 1993, Scotts Mills, Oregon, earthquake, *Geophysical Research Letters*, 22(1), 13–  
583 16.

584 Nabelek, J., Hetényi, G., Vergne, J., Sapkota, S.N., Kafle, B., Jiang, M., Su, H., Chen, J., Huang,  
585 B-S. and Hi-CLIMB team, 2009. Underplating in the Himalaya-Tibet Collision Zone Revealed  
586 by the Hi-CLIMB Experiment, *Science*, 325, 1371-1374.

587 Nakata, T., 1989. Active faults of the Himalaya of India and Nepal, *Geological Society of*  
588 *America Special Papers*, 232, 243-264.

589 Pandey, M.R., 1985. Seismic model of central and eastern lesser Himalaya of Nepal, *Journal*  
590 *of Nepal Geological Society*, 3(1-2), 1-11.

591 Pandey, M.R., Tandukar, R.P., Avouac, J.P., Lavé, J. and Massot, J.P., 1995. Interseismic strain  
592 accumulation on the Himalayan Crustal Ramp (Nepal), *Geophysical Research Letters*, 22,  
593 751-754.

594 Pandey, M.R., Tandukar, R.P., Avouac, J.P., Vergne, J. and Héritier, T., 1999. Seismotectonics  
595 of the Nepal Himalayas from a local seismic network, *Journal of Asian Earth Sciences.*, 17(5-  
596 6), 703-712.

597 Pearson, O.N. and DeCelles, P.G., 2005. Structural geology and regional tectonic significance  
598 of the Ramgarh thrust, Himalayan fold-thrust belt of Nepal, *Tectonics*, 24, TC4008, doi:  
599 10/1029/2003TC001617.

600 Robinson, D.M., DeCelles, P.G., Patchett, P.J. and Garzione, C.N, 2001. The kinematic  
601 evolution of the Nepalese Himalaya interpreted from Nd isotopes, *Earth and Planetary  
602 Science Letters*, 192, 4, 507-521, doi:10.1016/S0012-821X(01)00451-4.

603 Sapkota S.N. ,2011. Surface rupture of 1934 Bihar-Nepal earthquake: implications for seismic  
604 hazard in Nepal Himalaya, Ph.D thesis, Institut de Physique du Globe de Paris,France. pp 2-  
605 292.

606 Saul, J., Kumar, M.R. and Sarkar D., 2000. Lithospheric and upper mantle structure of the  
607 Indian shield, from receiver functions, *Geophysical Research Letters*, 27, 2357–2360.

608 Schmidt, D. A. and Gao, H., 2010. Source parameters and time-dependent slip distributions  
609 of slow slip events on the Cascadia subduction zone from 1998 to 2008, *Journal of  
610 Geophysical Research: Solid Earth*, 115, B00A18, doi:10.1029/2008JB006045.

611 Schulte-Pelkum, V., Monsalve, G., Sheehan, A., Pandey, M.R., Sapkota, S., Bilham, R. and Wu,  
612 F., 2005. Imaging the Indian subcontinent beneath the Himalaya, *Nature Letters*, 435,  
613 doi:10.1038/nature03678.

614 Schwartz, S. Y., Dewey, J. W. and Lay, T. 1989. Influence of fault plane heterogeneity on the  
615 seismic behavior in the southern Kurile Islands Arc, *Journal of Geophysical Research: Solid*  
616 *Earth*, 94(B5), 5637-5649.

617 Schwartz, S. Y. and Rokosky, J. M., 2007. Slow slip events and seismic tremor at  
618 circum-Pacific subduction zones, *Reviews of Geophysics*, 45(3).

619 Shrestha, A.B., Wake, C.P., Dibb, J.E, Mayewski, P.A., 2000. Precipitation fluctuations in  
620 Nepal Himalaya and its vicinity and relationship with some large scale climatological  
621 parameters, *International Journal of Climatology*, 20, 317 – 327.

622 Souloumiac, P., Leroy, Y.M., Maillot, B. and Krabbenhoft, K., 2009. Predicting stress  
623 distributions in fold-and-thrust belts and accretionary wedges by optimization, *Journal of*  
624 *Geophysical Research*, 114, B09404, doi: 10.1029/2008JB005986.

625 Stevens, V.L. and J.P. Avouac, 2015. Interseismic coupling on the main Himalayan thrust,  
626 *Geophysical Research Letters*, 42, 5828–5837, doi:10.1002/2015GL064845.

627 Szeliga, W., Melbourne, T., Santillan, M. and Miller, M., 2008. GPS constraints on 34 slow slip  
628 events within the Cascadia subduction zone, 1997–2005, *Journal of Geophysical Research:*  
629 *Geophysical Research*, v.110, *Solid Earth*, 113, B04404, doi:10.1029/2007JB004948.

630 Waldhauser, F. and Ellsworth, W.L., 2000. A double-difference earthquake location  
631 algorithm: method and application to the Northern Hayward Fault, California, Bulletin  
632 Seismological Society of America, 90 (6), 1353-1368.

633 Yatagai, A., Kamiguchi, K., Arakawa, O., Hamada, A., Yasutomi, N. and Kitoh, A., 2012.  
634 Aphrodite. Constructing a long-term daily gridded precipitation dataset for Asia based on a  
635 dense network of rain gauges, America Meteorological Society, Q07023, doi:  
636 10.1029/2011GC003513.

637 Zahradnik, J., Jansky, J. and Plicka, V., 2008. Detailed waveform inversion for Moment Tensor  
638 of  $M \sim 4$  events: examples from Corinth Gulf, Greece, Bulletin of the Seismological Society of  
639 America, 98 (6), pp. 2756-2771, doi: 10.1785/0120080124.

#### 640 **Table caption**

641 Table 1. Description of the main shocks of the three swarms of 1997. Origin time and  
642 epicentral location are from the NSC.

#### 643 **Figure captions**

644 Figure 1. Seismicity map of Central Nepal from the National Seismological Center of Nepal  
645 (Modified from Adhikari et al., 2015). Red dots are the aftershocks of the Gorkha earthquake  
646 and the yellow dots indicate epicenters prior to the Gorkha event since 1994. The iso-slip  
647 contours of the Gorkha earthquake are from Grandin et al., 2015. The black rectangle  
648 indicates the area used for Figure 2 and 4. Past earthquakes rupture areas (top right) from  
649 Bollinger et al., 2016. MFT: Main Frontal Thrust, MBT: Main Boundary Thrust, MCT: Main  
650 Central Thrust. The orange thin lines are the traces of the Southern Tibetan Grabens (Armijo  
651 et al., 1986)

652 Figure 2. Cumulative number of events during the interseismic period recorded by the NSC  
653 from 1994 to 2015 in the area delimited in Figure 1. The black line corresponds to the events  
654 of magnitude  $ML \geq 2.0$  scaled on the left side. The gray diamonds correspond to the events of  
655 magnitude  $ML \geq 4.0$  scaled on the right side. 30% of the events of  $ML \geq 4.0$  occurred in 1997.

656 Figure 3. Centroid Moment Tensor solution for the Sarshin earthquake occurred on January  
657 31<sup>st</sup> 1997. For each station, observations are shown with solid lines and synthetics with  
658 dotted lines. Z, R and T are the vertical, radial and transverse components respectively.  
659 Radial components of CHTO, HYB and WUS were discarded because of the high signal-noise  
660 ratio. 1 and 0 are the weights used in the inversion.

661 Figure 4. Spatial distribution of the seismic **episode** of 1996-1999, north of Kathmandu (see  
662 Figure 1): The map shows the relocated seismicity as a function of time and magnitude of  
663 Zone 1 and 2 (zones boundary: longitude  $85.4^\circ$ ). The main shock corresponds to the 1997  
664 January 31<sup>st</sup>  $ML=5.8$  ( $M_w 4.8$ ) earthquake **with the preferred focal mechanism plane in red**.  
665 The cross-sections include the relocated seismicity. A-A' and B'-B cross-sections are  
666 orientated N140 and N065, respectively. They stack seismicity located 10 km for A-A' and 3  
667 km for B'-B from each side of the track. **The area highlighted in light white correspond to the**  
668 **suspected fault segments at depth activated by the 1997 episode (see Figure 7 for**  
669 **interpretation).**The intersection between A-A' and B-B' cross-sections are indicated with a  
670 black cross. The green, blue and pink-brown lines at the bottom of the map are western,  
671 central and eastern respectively used in Figure 5.

672 Figure 5. Time sequence of the seismicity north of Kathmandu. The zones are indicated at  
673 the bottom of the map in Figure 4. The Sarshin earthquake is indicated by the yellow star.  
674 The red dashed line is the average rate of seismicity (108 events per year).

675 Figure 6. Spatio-temporal variations of the seismicity. A) Normalized time sequence of the  
676 midcrustal seismicity along the MHT. The curves correspond to the three swarm areas and  
677 the yellow one to the inter-swarms area. Gray shadow zone is the time covered in the map.  
678 B) Midcrustal seismicity for the period 1996-1997 in yellow, swarm seismicity in red.  
679 Orange circles are the Southern Tibetan Grabens north of the swarms.

680 Figure 7. Schematic evolution of the stress field and structure activation. A) Variation of  
681 shear stress and normal stress associated with a transient slip event on the Main Himalayan  
682 Thrust in a region with midcrustal tear faults and southern Tibetan grabens. The initial state  
683 is shown in black and is assumed tangent to the failure envelope represented by the straight  
684 line. 1, 2, and 3 refer to the different areas indicated in B and C. In area 1,  $s_1$  and  $s_3$  are  
685 horizontal, increasing and decreasing respectively, promoting failure. In area 2,  $s_1$  is  
686 horizontal, striking about north-south and increasing during interseismic deformation and  
687 transient slip events, promoting failure. In area 3,  $s_3$  is horizontal, striking approximately  
688 east-west and decreasing during interseismic deformation, promoting failure. B) and C)  
689 Kinematical evolution north of Kathmandu in 1996-1997; orange surface corresponds to the  
690 area with a coupling  $>50-80\%$  depending on source (Ader et al., 2012; Grandin et al., 2015).  
691 B) Static stress change induced by slip on the tear fault is schematized by Coulomb stress  
692 lobes, respectively blue and red for  $DCFF < 0$  and  $> 0$ . Dotted lines and filled areas correspond  
693 respectively to the  $DCFF$  calculated for receiver faults with the backthrust and the thrust  
694 orientation (more information in Table S1, Table S2, and Figure S8 to S11). C) Activation of  
695 the backthrust (in green) and the thrust fault (in salmon) as a consequence of static stress  
696 change induced by the tear fault (B). D) Schematic three dimensional block, with vertical  
697 exaggeration, of the MHT with the backthrust (green) and the tear fault (purple). Colors on  
698 the MHT correspond to the coupling: red: total coupling ( $>50-80\%$ ), orange: transition zone

699 (60%-40%), Yellow: completely decoupled (0%) (Ader et al., 2012; Grandin et al., 2015).

700 White arrows show the kinematics of the structures.

701

702

703



23 At its eastern end, the midcrustal cluster is offset by 20 km to the south suggesting the  
24 presence of a tear fault. The analysis of the time sequence allows constraining a scenario  
25 involving stress transfer between these local midcrustal structures, beginning more than one  
26 month before the 1997 main shock. The temporal evolution of the seismicity is strikingly  
27 similar for two other transient seismic swarm episodes which developed hundreds of  
28 kilometers apart along the Main Himalayan Thrust at the same time. The local stress field  
29 appears responsible for the higher sensitivity of these regions to subtle strain transients  
30 developing along the Main Himalayan Thrust.

31 **Key words:** seismicity, Main Himalayan Thrust, fault segmentation, relative relocation.

32

33

34

35

36

37

38

39

40

41

42

43

44

45 **1. Introduction**

46 Along-strike variations of seismic activity on a fault can result from lateral variations in the  
47 geometry of the locked fault zone, spatial heterogeneity in frictional parameters or from  
48 unsteady loading during the interseismic period. Variations in seismicity rates along the  
49 downdip end of a locked megathrust may reveal that the structure is segmented, and these  
50 segment boundaries may correspond to the barriers that delimit major seismic ruptures (e.g.  
51 Schwartz et al., 1989; Collot et al., 2004; Métois et al., 2012; Holtkamp et al., 2011;  
52 Holtkamp and Brudzinski, 2011). The Main Himalayan Thrust (MHT) fault in Nepal qualifies  
53 as one interesting fault to document in terms of seismicity variations given its seismogenic  
54 potential and the possible control of the coseismic ruptures by persistent structural features  
55 (e.g. Grandin et al., 2015). Indeed, despite the apparent homogeneity of the stress build up  
56 revealed by geodesy (Ader et al., 2012; Stevens and Avouac, 2015) significant variations of  
57 the seismic rate have been reported along strike (Pandey et al., 1999). Some of the  
58 variations in seismic rate are persistent in time and might reveal lateral heterogeneity in  
59 terms of seismic coupling and/or tectonic structures along strike of the MHT. Others are  
60 temporary, related to transient episodes including swarm activity or mainshock-aftershock  
61 sequences.

62 On April 25 2015 at 11h56 Nepal Standard Time (06h11 UTC), the Mw 7.8 Gorkha  
63 earthquake ruptured a 120 km-long and 35-50 km wide fault segment of the MHT (e.g.,  
64 Avouac et al., 2015; Grandin et al., 2015; Kobayashi et al., 2015; Elliott et al., 2016)(Figure 1),  
65 abutting the great M8.2 1934 earthquake rupture. The propagation of the rupture and the  
66 slip along the fault plane were heterogeneous, leading some authors to suggest possible

67 along strike variations of the structure at depth (Grandin et al., 2015, Fan and Shearer,  
68 2015).

69 The aftershocks near the trace of the rupture in the vicinity of Kathmandu are  
70 heterogeneously distributed (Adhikari et al., 2015; Bai et al., 2015). Some aftershocks are  
71 clustered under Kathmandu valley, a place where no seismicity has been observed during  
72 the interseismic period (Figure 1). In the meantime, north of the Nepalese capital, the  
73 aftershocks epicenters coincide with the location of the midcrustal interseismic cluster (10-  
74 20 km depth) (Figure1). The heterogeneous distribution of the Gorkha earthquake  
75 aftershocks and the seismicity during interseismic period north of Kathmandu could be due  
76 to structural complexities or a transient event. The goal of our study is to use small  
77 earthquakes prior to the 2015 Gorkha event to resolve structural and frictional  
78 characteristics that might control the rupture parameters of the main shock.

79 In order to test such a hypothesis, we analyze the spatio-temporal variations of the  
80 seismicity during the interseismic period north of Kathmandu, a region well covered by the  
81 Nepalese national seismological network. We first relocate the seismic events using a  
82 double-difference algorithm (Waldhauser and Ellsworth, 2000) and perform a Centroid  
83 Moment Tensor inversion of the largest instrumentally recorded event in the region, ML=5.8  
84 on January 31<sup>st</sup> 1997. We then interpret the spatial pattern of seismicity in terms of  
85 geological structures at depth, and finally focus on the temporal variation of the seismicity  
86 rate along this structure.

## 87 **2. Data description**

### 88 **2.1. Regional Network**

89 The seismicity of central and eastern Nepal has been continuously monitored since the  
90 1990s by the National Seismological Centre of Nepal (NSC) with a national network  
91 composed of 21 short period vertical component seismic stations. Among them 12 high gain  
92 stations have been operational since 1994 in central and eastern Nepal providing a  
93 completeness of the seismic catalogue for that region around local magnitude  $ML=2.0$   
94 (Pandey et al., 1999). Their records are processed using Jade-Onyx acquisition-treatment  
95 software in which a 1D velocity model is used to locate earthquakes using the phases picked  
96 manually at NSC (Pandey, 1985; Pandey et al., 1995, Adhikari et al., 2015). A complementary  
97 network of 3 stations was deployed temporarily, from July 1995 to December 1996. The  
98 addition of these stations facilitated improved locations for the small earthquakes generated  
99 at midcrustal depths below the front of the high topography (Cattin and Avouac, 2000) in the  
100 vicinity of the Main Himalayan shear zone (Nabelek et al., 2009).

## 101 **2.2. Earthquake catalogue**

102 North of Kathmandu, the interseismic activity appears concentrated at midcrustal depths  
103 within a permanent seismic cluster (Pandey et al., 1995; Cattin and Avouac, 2000) (Figure 1)  
104 modulated by a few transient seismicity bursts (Figure 2). The most important seismicity  
105 burst was recorded in 1997. Indeed, 30% of the  $ML \geq 4.0$  events of the catalogue in this  
106 region occurred in that year (Figure 2). The sequence culminated after the occurrence of the  
107 “Sarshin earthquake” an  $ML=5.8$  event which happened on January 31<sup>st</sup> 1997 (Table 1), an  
108 event preceded 3 hours before by a foreshock of  $ML 5.1$ . This event resulted in a maximum  
109 shaking intensity of  $MMI VII$  and was felt in Kathmandu 40 km SE from its epicenter. It  
110 caused significant impact ( $MMI VI$ ) over a region  $1800 \text{ km}^2$  in size (Sapkota, 2011). Given its  
111 magnitude, this event was also recorded at teleseismic distances by international

112 institutions, which assigned a body-wave magnitude (mb) around 5.2 and depths between  
113 17 and 23 Km (Table 1).

114 The Sarshin earthquake was followed by more than 160 aftershocks in a region spanning 50  
115 x 30 km<sup>2</sup>, a surface significantly larger than the expected rupture extension. The orientation  
116 of the seismic cluster based on NSC locations is unclear and we expect that relocated  
117 aftershocks will help to constrain the geometry of the structure activated by the Sarshin  
118 earthquake.

### 119 **3. Method**

#### 120 **3.1. Centroid Moment Tensor at regional scale**

121 Seismic data of the 1997 Sarshin earthquake recorded by stations at distances up to 1700 km  
122 and of good quality are used to calculate a Centroid Moment Tensor. This includes data from  
123 stations LSA (Tibetan plateau), HYB (central India), WUS (northern China) and CHTO  
124 (Thailand) (Figure 3).

125 The centroid moment tensor solution is retrieved from the inversion of regional long-period  
126 seismic waves (40-100s). The procedure is taken from Nábelek (1984) and is adapted to a  
127 low-frequency inversion (Nábelek and Xia, 1995). For the centroid moment tensor inversion,  
128 a 1-D velocity structure should be chosen to compute synthetic Green's functions and model  
129 the observed waveforms at seismic stations. Processing a large number of events (29  
130 earthquakes in (Burtin, 2005) and 107 earthquakes in (Baur, 2007) in the Himalaya and  
131 Tibetan Plateau regions) we failed to correctly invert the seismic waveforms at stations with  
132 a single velocity model. Seismic signals from sources occurring along the Himalayan arc were  
133 recorded at stations located around the Tibetan plateau and the India plate. Therefore,  
134 velocity structures through which seismic waves travel can drastically change. For instance

135 when a velocity model with a Moho depth fixed at 35 km (ex. India path) is used, the  
136 modeled waveforms for northern Tibetan stations will systematically arrive sooner than the  
137 observed ones. To overcome this issue, each ray path is associated with a specific 1-D  
138 structure. For the Indian station HYB, the model is from Saul et al., (2000) with a Moho  
139 depth at 35 km. For the Tibetan station LSA and northern China station WUS, the model is  
140 modified from Haines et al., (2003) with a Moho depth at 65 km. In this latter model, we had  
141 to remove the 5 km thick sedimentary layer because otherwise the synthetic inverted  
142 seismic waves were delayed too much. Finally, the model for the Thai station CHTO was set  
143 to an intermediate model between the Indian and Tibetan models with a Moho depth at 45  
144 km. These velocity models were tested using a trial and error procedure on the 29 focal  
145 mechanisms studied (Burtin, 2005); we retained those models that resulted in synthetics  
146 that best matched the observed seismic data (Figure 3) – See Burtin, 2005 for further  
147 information. Furthermore, for each earthquake analyzed in Burtin (2005), including the  
148 Sarshin earthquake, the centroid moment tensor source depth was constrained through a  
149 grid search algorithm that minimized the waveform misfit, using at first a coarse step size (10  
150 km) followed by a finer step size (1 km).

### 151 **3.2. Relative relocation at local scale**

152 We calculate relocations using the double-difference algorithm HypoDD (Waldhauser and  
153 Ellsworth, 2000) for the seismicity clustered north of Kathmandu, in the trace of the Gorkha  
154 earthquake. We use data from the NSC bulletin for the period 1996-1999 and the whole  
155 bulletin from the temporary experiment of 1995-1996. Relative locations are resolved by  
156 solving an inverse problem using a damped least-square technique, minimizing the residuals  
157 between observed and calculated phase delay times between a pair of adjacent earthquakes

158 recorded at common stations. This procedure reduces the biases induced by velocity model  
159 errors along the paths from hypocenters to seismic stations. The velocity model considered  
160 hereafter is the 1-D model of Pandey (1985) with a  $V_p/V_s$  of 1.73. We initially attribute to  
161 each seismic event the origin time and hypocenter of the NSC seismic bulletin. We also  
162 allocate location errors corresponding to the average of the longitudinal and latitudinal  
163 uncertainties as well as depth uncertainties documented in the bulletin. Undetermined  
164 depths in the database are fixed to 0. The second set of inputs include the arrival times of P  
165 and S phase arriving at a station for a given event. The weight for the P phases is fixed to 1  
166 and for the S phases to 0.3.

167 Given the very high density of events located immediately in the vicinity of the Sarshin  
168 earthquake, compared to the more diffuse spatial and temporal pattern of the seismicity  
169 elsewhere, we divide the catalogue of events in two, a western and an eastern region  
170 (respectively zones 1 and 2 hereafter) separated at 85.4E (Figure S1 and S3). This division will  
171 enable us to better optimize the relocation process.

172 We select pairs of phases at every station considering (1) a maximal separation between  
173 hypocenters of 20 km and (2) a minimum number of links between two neighbor events of 8  
174 for Zone 1 and of 4 for Zone 2.

175 The relocation is performed in both cases with P and S phases when available and with three  
176 sets of iterations taking into account the seismic bulletin parameters. We set the damping at  
177 20 in a LSQR inversion. The first set iterates four times using only P waves. The second set  
178 iterates also four times with P and S waves. The third set iterates 8 times taking into account  
179 P and S waves, limiting the residuals to 5 seconds and the maximum distance between linked  
180 pairs to 10 km. The relocation of Zone 1 considers 8 as the minimum number of links per pair

181 to form a continuous cluster. There is no clustering a priori parameter for the relocation of  
182 Zone 2.

183 We tested the most influential parameters for both the pair-phase selection and the  
184 relocation process. In the pair-phase selection, we tested values at 4, 8, and 12 for the  
185 minimum number of links between two neighbor events. We also tested maximum  
186 separation between hypocenters at 20 and 50 km. The number of pair-phases created  
187 increase considering either a larger number of minimum links per pair or a larger maximum  
188 separation distance between hypocenters, however there are more events weakly linked.  
189 The minimum number of links between two neighbor events tested changes in Zone 1 and 2  
190 because of the density of events. We also tested various numbers of iterations (4 and 8 for  
191 each set) in the relocation process. The RMS misfit decreases for the first two sets until it  
192 stabilizes after 4 iterations. The solution becomes unstable with 8 iterations, resulting in a  
193 centroid shift and in an unstable RMS misfit. In the third step, 8 iterations are needed to  
194 stabilize the RMS misfit. Geometrically, the relative relocations were similar for any iteration  
195 scheme.

196 The tests results support the parameters we chose for Zone 1 and 2.

#### 197 **4- Results**

198 In Zone 1 (Figure 4), the seismic bulletin includes 230 events with 2408 phases from which  
199 20140 P-phases pairs and 12469 S-phase pairs are found. 80% of P-phase pairs and 84% of S-  
200 phase pairs are selected. The event pairs have an average of 10 links with an average offset  
201 of 6.04 km. After event pair selection, 167 events are successfully relocated, with less than  
202 1500 m of 2-sigma-relative location errors in x, y, z and a RMS misfit reduction of 60%  
203 (Figure S2, S3, S5, and S6).

204 The seismic bulletin covering Zone 2 (Figure 4) includes 548 events with 4886 phases from  
205 which 45938 P-phase and 39002 S-phase pairs are determined. Respectively, 49% and 45%  
206 of P- and S-phase pairs are selected. The event pairs have an average of 6 links with an  
207 average offset of 6.9 km. 477 events are selected, from which 384 events are successfully  
208 relocated with less than 100 m of 2-sigma-relative location errors in x, y, z. The RMS misfit  
209 reduction, following the integration of the phases picked at the temporary 3 component  
210 stations, is close to 90% (Figure S2, S3, S4, S5, S6, and S7).

211 The relocation of Zone 1 and Zone 2 seismicity indicates the presence of two separate  
212 clusters during the 1997 seismic episode (Figure 4). The westernmost seismic cluster is  
213 located between  $85.3^\circ$  and  $85.4^\circ$ , covering an area of  $7 \times 11 \text{ km}^2$  (Figure 4, map), just above  
214 the January 31<sup>st</sup> Sarshin earthquake hypocenter (Figure 4, cross-section). The visual  
215 inspection of 3D plots shows that the seismicity lies on a plane that strikes  $N050 \pm 20 \text{ E}$   
216 dipping steeply southeast ( $70\text{-}80^\circ$ ). The other seismic cluster is smaller ( $6 \times 8 \text{ km}^2$ ) and is  
217 located between  $85.4^\circ$  and  $85.5^\circ$ . It describes an almost vertical plane striking  $N155 \pm 20 \text{ E}$   
218 (Figure 4). No large event is associated with this cluster. The remaining relocated seismic  
219 events do not show a particular geometry. Most of them are located in a 10 km-wide band  
220 east of  $85.5^\circ$ .

221 The centroid moment tensor solution for the January 31<sup>st</sup> Sarshin earthquake indicates a  
222 best centroid depth at 17 km and a reverse motion with a slight strike-slip component. One  
223 nodal plane (NP1) strikes  $N075$  and dips  $85^\circ \text{SE}$ , and the second (NP2) strikes  $N152$  and dips  
224  $24^\circ \text{NE}$ . Although it is difficult to quantify uncertainties on the centroid moment tensor  
225 solution, the azimuthal coverage being decent and the changes in centroid moment tensor  
226 being small in the vicinity of the best depth, we consider the uncertainties to be moderate

227 (+/-20°) (Zahradnik et al., 2008). In particular NP1, which dips at a high angle, is quite stable  
228 in the inversions. The NP1 plane is the closest to the plane defined by the relocated  
229 aftershocks of the Sarshin earthquake. The moment magnitude obtained is  $M_w=4.8$ .

230 The depths of the relocated events range from 15 to 26 km in the western cluster, with the  
231 main shock at 24 km depth which is slightly deeper than previous determinations (Table 1).  
232 NSC gives a hypocenter at 20.3 km while the centroid moment tensor centroid depth is at 17  
233 km. Although the relocation allows us to place constraints on the relative positions of  
234 hypocenters leading to a fairly well defined geometry for the cluster, the centroid depth of  
235 the cluster (~22 km) is less well constrained as the closest station that recorded these events  
236 is located at ~ 25 km, and thus the centroid could move by a few kilometers. Both  
237 hypocenter depths and centroid moment tensor centroid depths being within +/-5 km, we  
238 think the differences may not be significant. In addition, as most crustal earthquakes  
239 nucleate at depth and propagate towards the surface (e.g., Das and Scholz, 1983; Huc et al.,  
240 1998), we expect the hypocenter depth of the mainshock to be larger than its centroid  
241 moment tensor depth. This will be particularly true if the co-seismic slip is small and the  
242 ruptured area large for a  $M_w4.8$  event. Indeed, the source of a  $M_w4.8$  can be either  $2 \times 2 \text{ km}^2$   
243 with 10cm of slip or  $5 \times 5 \text{ km}^2$  with 2 cm of slip.

## 244 **5- Interpretation**

### 245 **Spatial distribution of the Sarshin Swarm**

246 Most of the 1996-2000 Sarshin Swarm seismicity is located at midcrustal depths, with  
247 centroid depths at 22 and 15 km respectively for the two clusters (Figure 4). These depths  
248 roughly correspond to the depth of the Main Himalayan shear zone, as interpreted on

249 images obtained along profiles based on receiver function analysis (Schulte-Pelkum et al.,  
250 2005; Nabelek et al., 2009; Duputel et al., 2016).

251 The westernmost cluster develops after the main shock of the Sarshin earthquake over a 7 x  
252 11 km<sup>2</sup> region. Given the geometry of the cluster and the fault plane solution parameters of  
253 its main shock, the January 31<sup>st</sup> 1997 Sarshin earthquake, we associate this seismic swarm to  
254 the activation of a NE-SW backthrust, steeply dipping to the southeast. Assuming that the  
255 aftershock distribution corresponds to the maximum extent of the fault segment ruptured  
256 by the main shock, a Mw 4.8 ( $M_0 = 2.3 \cdot 10^{16}$  Nm deduced from the centroid moment tensor  
257 determination), and assuming a shear modulus of 32 GPa we obtain an average minimum slip  
258 of 1 cm. Considering that aftershocks may more likely extend beyond the edges of the  
259 ruptured plane, its surface is likely overestimated. A surface overestimation by 100% will  
260 lead to doubling the average slip, at 2 cm. This amount of slip at depth induces infra-mm  
261 displacements at the surface GPS sites around, values below the resolution capacity of the  
262 campaign GPS available at that time (Jouanne et al., 2004).

263 A rupture on a steep south-eastward dipping - northwestward verging thrust at mid-crustal  
264 depths below the front of the high topography may correspond either to the activation of (a)  
265 a fault segment at the forelimb of the lesser Himalayan duplex (e.g. Pearson and DeCelles,  
266 2005; Khanal and Robinson, 2013), or (b) a local shear zone within the hinge above the flat-  
267 decollement/ramp, as predicted by mechanical models (Souloumiac et al., 2009) (Figure 7D).  
268 We prefer the latter interpretation, as the depth seems more consistent with the downdip  
269 end of a midcrustal ramp than the passive roof-thrust of the duplex.

270 The relocated seismicity appears offset by 20 km from west to east, describing an eastward  
271 right-stepping strand. Note that this step is not an artifact due to the location of the

272 boundary between the two zones considered in the relocation process: alternative  
273 relocations considering only one zone, keeping the same relocation parameters, produced  
274 similar spatial patterns, with the seismic cluster stepping to the south in this area. This offset  
275 could be explained by the presence of a tear fault between two ramps or structural  
276 discontinuities within the Main Himalayan shear zone such as a stepover of the fault. We  
277 prefer the former hypothesis given the absence of overlapping seismicity along strike. In  
278 addition, the vertical NW-SE plane described by the second cluster (85.4° and 85.5°)  
279 identified in the relocation results is consistent with tear faulting although we could not  
280 compute any fault plane solution to prove this. Such tear faults are required because of the  
281 topology of the MHT flat/ramp system and its lateral variations (Figure 7). The right lateral  
282 tear fault suspected to develop at depth within the trace of the second cluster is aligned  
283 with an active dextral fault system reaching the surface along the 20 km-long NNW-SSE Jhiku  
284 Kholā fault (Kumahara et al., 2016).

285 We propose that the backthrust and tear fault activated during the 1997 seismic episode,  
286 and in a more general way every significant variation of the structure at depth along the  
287 MHT, might influence its behavior. It could affect the propagation of the co-seismic rupture  
288 (e.g. Béjar-Pizarro et al., 2010), influencing the co- and post-seismic slip distribution as well  
289 as the location of the aftershocks. Note that the structure we studied is located in between  
290 two patches of maximum slip of the Gorkha earthquake proposed by some authors (e.g.  
291 Avouac et al., 2015; Grandin et al., 2015) (Figure 1).

## 292 **Temporal distribution of the seismicity at local and regional scales**

293 The time structure of a seismic episode gives a dynamic sense and evolution of the  
294 phenomenon that the spatial distribution does not. Both are essential to interpret our  
295 results.

296 The time structure of the seismicity in this area (Figure 4) exhibits complex variations in the  
297 period covered by our study. The seismicity rate decreases first in mid-1996 (Figure 2 and 5).  
298 This relative quiescence is difficult to ascertain, being concurrent with the monsoon arrival, a  
299 period during which the seismic noise level and therefore the completeness magnitude of  
300 the catalogue is higher than on average, a period during and slightly after which the seasonal  
301 load of the India plate has a genuine influence on the seismicity (Bollinger et al., 2007;  
302 Bettinelli et al., 2008; Burtin et al., 2008). The seismic rate remains low until December, far  
303 after the monsoon period, and is followed by a sharp increase. The seismic events are then  
304 clustered between  $85.4^{\circ}$  and  $85.5^{\circ}$  (Central zone in Figure 4), mostly along a 6 km-long  
305 vertical plane oriented N155. This activity, decreasing at the beginning of 1997, is followed  
306 by the development of another cluster 15 km to the northwest in January (Figure 4, 5). The  
307 swarm in the area begins before the Sarshin main shock which occurred at 20:02 (local time)  
308 on January 31st and was preceded by a ML5 and smaller events a few hours earlier. The  
309 seismic cluster that developed within the next three months within 10 km from the  
310 hypocenter is typical of an aftershock sequence. In the meantime, the seismicity rate east of  
311  $85.5^{\circ}$ E increased significantly (Figure 5).

312 Surprisingly, this unusual transient seismic activity is not exceptional in the Himalaya region.  
313 Indeed, in eastern Nepal, a seismic swarm developed between  $86.8$  and  $87^{\circ}$ E, generating 80  
314 events south of Mount Everest, between November 1996 and May 1997. No main shock was  
315 detected prior to the onset of the seismic swarm but a larger shock, with a ML 5.8, occurred  
316 on the 30/12/1996 (Table 1) and was followed by aftershocks (Figure 6). In western Nepal,

317 between 80.5° and 81°E, a similar swarm developed with a main shock on 05/01/1997 of  
318 ML=6.3 (Table 1).The location of the seismicity in these two areas is not sufficiently resolved  
319 to perform an analysis similar to what has been done here. The time structure of these two  
320 swarms is very similar to that of Sarshin as illustrated on Figure 6.

321 Altogether, the 3 clusters contribute to 40% of the yearly midcrustal events detected along  
322 the front of the range in Nepal. Their cumulative along strike development accounts for ~ 10  
323 % of the length of the midcrustal cluster making this event the most important seismicity  
324 burst of the interseismic period recorded by the Nepal National Seismological Network. No  
325 significant seismic rate variations were detected in between the three clusters (Figure 6).

## 326 **6- Discussion**

327 Complex spatial and temporal variations of seismicity have been revealed at local and  
328 regional scales. Locally, north of Kathmandu, the spatial distribution of the seismicity  
329 coincides with a back-thrust and a thrust segment separated by a proposed 20 km-long tear  
330 fault. Their consecutive activation follows the development of a seismic swarm on the tear  
331 fault. The geometry of the fault system is consistent with a right lateral slip on the tear fault.  
332 This scenario is compatible with the topology of the thrust system as well as with the  
333 kinematics of the dextral NNW-SSE Jhiku Khola fault described in continuity to the south  
334 (Kumahara et al., 2016). The en-echelon segments of the MHT there are close to the  
335 unstable-stable transition zone USTZ (e.g. Jackson and Bilham, 1994; Bettinelli et al., 2006).  
336 This behavior was confirmed recently by the determination of the seismic coupling that falls  
337 there between 0.4 and 0.6 (Ader et al., 2012; Grandin et al., 2012; Stevens and Avouac,  
338 2015).

339 The seismic activity in 1997 in this region could result from (1) a local unsteady loading or (2)  
340 a local strain transfer in the vicinity of the USTZ. However, rather than just a local strain

341 transient, the development in 1996-97 of 2 other clusters hundreds of kilometers apart,  
342 depicting similar temporal variations, may imply (3) a large scale unsteady loading. The  
343 unsteady loading could be due, among others, to a lithospheric response to the water mass  
344 redistribution after the monsoon or to a slow slip event. However, in 1996, the precipitation  
345 records were fairly typical (e.g., Shrestha et al., 2000; Yatagai et al., 2012). This leads us to  
346 propose that the 1997 seismic episode may be related to a slow slip event. A transient slip  
347 event with a slip amplitude of tens of centimeters is precluded due to the absence of  
348 measurable changes in the seismicity rate between the clusters (Figure 6A). Indeed, a  
349 seismicity change would likely occur after a centimetric to decimetric scale slow slip event,  
350 which would in turn release years of stress build up and therefore most probably induce  
351 years of midcrustal seismicity along strike. The lower end of the slip amplitude expected, i.e.  
352 1 cm, would correspond roughly to the seismic slip accommodated during the Sarshin  
353 earthquake (see previous section for estimation). In Sarshin area, such an amount of slip at  
354 midcrustal depths generates only infra-millimetric displacements at RAM0 and SYA0,  
355 regional GPS stations respectively 17 and 20 km from the updip-end of the ruptured fault  
356 plane. These stations were surveyed briefly in 1995 and 1998 (1 to 4 days/sessions). They  
357 were translated in 3 years by  $19 \pm 6$  mm and  $21 \pm 7$  mm respectively in an India fixed reference  
358 frame (Jouanne et al., 2004). The large uncertainties of the measurements preclude  
359 resolving the infra-millimetric displacements induced by the Sarshin earthquake as well as  
360 those induced by any strain transient with similar amplitudes. We further note that the  
361 displacements uncertainties for both stations amounts to one third of the measurements, a  
362 value comparable to one year of strain above the Main Himalayan Thrust. The thrust  
363 accommodates, at depth, on average, a shortening of 18 mm/yr (Ader et al., 2012).  
364 Detecting a transient slip event at depth on the creeping part of the MHT of less than 18 mm

365 therefore seems impossible. This result is corroborated by the absence of any major change  
366 in the shortening rates estimated elsewhere in Nepal by campaign GPS data, and by the  
367 continuous DORIS time series available at Everest.

368 Several of the large transient events elsewhere in the world were accompanied by tremors  
369 and low frequency earthquakes (Schwartz and Rokosky, 2007). Such kinds of seismic events  
370 have not been observed in 1997 in Nepal, a period during which the continuous seismic  
371 signals recorded by National Seismological Network was not stored. Further analysis of these  
372 signals to detect tremors or low frequency earthquakes is therefore limited to the cut signals  
373 of seismic events which, according to a preliminary analysis, present a typical spectra.

374 Despite the lack of direct evidence that tremors and low frequency earthquakes occurred,  
375 we think the seismic catalogue contains other indirect evidences of this process.

376 A subtle transient slip event may generate heterogeneous seismicity along strike due to the  
377 geometry and state of stress changes along strike of the MHT. Indeed, the midcrustal  
378 seismicity under the front of the Himalayas appears sensitive to the local state of stress  
379 which depends mainly on the regional tectonic stress and the topography, through their  
380 influence on the preferred orientation of the failure planes (Bollinger et al., 2004a). In  
381 between the Main Frontal Thrust and the front of the High range, S3 and S1, the minimal  
382 and maximal principal stresses, are respectively vertical and north-south. S1 increases during  
383 interseismic deformation due to slip at depth on the MHT, promoting failure on EW striking  
384 thrust planes (Figure 7A(area 2)). Further north, in the Southern Tibetan grabens (Figure 6B),  
385 S1 is vertical while S3 is horizontal, striking approximately east-west. S3 might decrease  
386 during interseismic deformation (Figure 7A(area 3)), since east-west extension increases in  
387 the Southern Tibetan Graben due to the divergence of thrusting along the Himalayan Arc  
388 (Bollinger et al., 2004a). This promotes failure on north-south oriented normal faults (ie: the

389 southern Tibetan grabens). In between these two domains (i.e. south of the range, Tibetan  
390 Plateau: between area 2 and 3 on Figure 7A) the regional state of stress might promote the  
391 existence of NW-SE and NE-SW strike slip faults. This is valid for a range of depths in the  
392 cluster which depends on both  $S_1$  and  $S_3$  and the local non compensated topography. In this  
393 area, the intermediate stress component is vertical, while the maximum and minimum  
394 principal stresses correspond respectively to the north-south and east-west stress values  
395 (Figure 7A(area 1)). The strike slip faults in this region are very sensitive to the simultaneous  
396 N-S and E-W stress variations (Figure 7A). The lack of strike slip Centroid Moment Tensor  
397 solutions for intermediate events ( $M > 5.5$ ) during the last decades along the Himalaya  
398 demonstrate that strike slip faulting is infrequent along strike, probably due to the  
399 restriction to a small depth range of the corresponding state of stress. Besides the presence  
400 of large scale active strike-slip faults affecting the lesser Himalayas (Nakata, 1989),  
401 interpreted as resulting from large scale strain partitioning (Nakata, 1989; Murphy et al.,  
402 2014) or from the presence and migration of lateral ramps (Bollinger et al., 2004b), few  
403 active strike-slip fault segments were described at the foot of the High range (Nakata, 1989).  
404 However, tear-faults are suspected at midcrustal depths because of the lateral variations of  
405 the midcrustal ramps along the strike of the Main Himalayan thrust (e.g. Robinson et al.,  
406 2001; Bollinger et al., 2004b; Grandin et al., 2012). Despite the publication of balanced cross  
407 sections immediately west of Sarshin area (e.g. Pearson and Decelles, 2005; Khanal and  
408 Robinson, 2013), the present-day positions of the midcrustal ramps in the vicinity of the  
409 seismic cluster studied here are still unresolved. Assuming the cluster represents the edge of  
410 the MHT locked segment (e.g. Cattin and Avouac, 2000; Bollinger et al., 2004; Ader et al.,  
411 2012, Grandin et al., 2015), a dextral NW-SE transform structure is required for the sake of  
412 geometrical continuity (Figure 4 and 5, Central zone in blue). Assuming that this swarm is

413 located on such a right lateral strike slip segment, its activity in December 1996 creates static  
414 stress changes at its extremities. It leads to the generation of 2 positive Coulomb stress  
415 variations ( $\Delta CFF$ ) lobes on its NW and SE sides (while NE and SW would see a negative  
416  $\Delta CFF$ ) (Figure S8 to S11 and Table S2). This static stress change scenario accounts for the  
417 generation of seismicity along the backthrust to the NW and the thrust to the SE as well as  
418 with the lack of microseismic activity along its NE and SW extremities (Figure 7B and 7C).  
419 Furthermore it is consistent with Sarshin focal mechanism depicting a NE-SW oriented fault  
420 plane solution (Figure 4).

421 Whether similar kinematics and mechanisms are involved in the generation of the Far  
422 western and eastern Nepal seismic swarms is unknown. Unfortunately, the seismicity in  
423 these regions cannot be analyzed with a similar relocation approach due to the less optimal  
424 geometry of the seismic network and completeness of the database. But the 3 swarms are  
425 located in similar settings, within the midcrustal cluster at similar distances from the USTZ  
426 and within the trace of southern Tibetan Grabens (Figure 6B). Another similarity is their time  
427 sequence that begins with a weak but detectable decrease of seismicity prior to the swarms'  
428 development (Figure 6A). These rate decreases begin about 6 months prior to each swarm,  
429 during the onset of the monsoon. That the higher level of seismic noise during the monsoon  
430 is responsible for the seismic rate decrease is possible (Bollinger et al., 2007), but the rate  
431 remains low after the end of the monsoon and the decrease of the seismic noise generated  
432 by landsliding and rivers (Burtin et al., 2008). An alternative interpretation could be that the  
433 seismicity was partially inhibited and then promoted due to the response of the crust to a  
434 loading/unloading of continental water (Bettinelli et al., 2008; Chanard et al., 2014) in 1996.  
435 Whatever the scenario, the simultaneous development of these swarms may have resulted  
436 from a transient slip event similar to those detected along other subduction zones (e.g.

437 Cascadia, Mexico, Japan,...) with an affected area between 30 to 600 km along strike, and  
438 transient slip lasting 6 days to about a year with amplitudes between 5 mm and 5.6 cm (e.g.  
439 Dragert et al., 2001; Schmidt and Gao, 2010; Schwartz and Rokosky, 2007; Szeliga et al.,  
440 2008).

441 Such a slow slip event occurring on the Main Himalayan Thrust could play a role in the  
442 seismic cycle of the locked segment of the fault. Indeed, such transient events bring the  
443 locked fault zone closer to failure by several months (Dragert et al., 2001), besides the  
444 interseismic loading on the fault.

#### 445 **7- Conclusion**

446 The first conclusion to be drawn from this work is that the downdip end of the locked  
447 section of the Main Himalayan Thrust exhibits lateral seismicity variations that may reveal  
448 the presence of structural complexities at midcrustal depths. The right-stepping geometry of  
449 the seismicity, north of Kathmandu, is interpreted as resulting from the activation of a tear  
450 fault between a backthrust and a thrust segment. This structural complexity might have  
451 influenced the slip distribution during the Gorkha earthquake rupture as revealed by a local  
452 minima in the region of high slip of some published slip models. A second major conclusion  
453 is that the time sequence of the seismic swarm which developed there in 1996-97 is  
454 consistent with a propagation of a local strain transient, from the tear fault to the backthrust  
455 and thrust. Finally, the temporal coincidence between this swarm and two others at far  
456 distances leads us to suspect the development of a larger-scale transient slip event on the  
457 Main Himalayan Thrust. The local stress field appears responsible for the higher sensitivity of  
458 these areas to strain transients and needs therefore to be monitored to ascertain the  
459 presence of infrequent subtle slow slip events along the Himalaya.

#### 460 **Acknowledgements**

461 This project is funded by the French Agence Nationale de la Recherche (ANR-13-BS06-0006-  
462 01) and the Commissariat à l’Energie Atomique et aux Energies Alternatives. We thank the  
463 National Seismological Centre, Sudhir Rajaure and Soma Nath Sapkota for early exchanges  
464 on the seismic catalogue and macroseismic field of the Sarshin earthquake. The authors also  
465 thank the two anonymous reviewers and Gavin P. Hayes for their helpful comments that  
466 improved the paper.

#### 467 **References**

468 Ader, T., Avouac, J.P., Liu-Zeng, J., Lyon-Caen, H., Bollinger, L., Galetzka, J., Genrich, J.,  
469 Thomas, M., Chanard, K., Sapkota, S.N., Rajaure, S., Shrestha, P., Ding L. and Flouzat, M.,  
470 2012. Convergence rate across the Nepal Himalaya and interseismic coupling on the Main  
471 Himalayan Thrust: Implications for seismic hazard, *Journal of Geophysical Research*, 117,  
472 B04403, doi: 10.1029/2011JB009071.

473 Adhikari, L.B., Gautam, U.P., Koirala, B.P., Bhattarai, M., Kandel, T., Gupta, R.M., Timsina, C.,  
474 Maharjan, N., Maharjan, K., Dahal, T., Hoste-Colomer, R., Cano, Y., Dandine, M., Guilhem, A.,  
475 Merrer, S., Roudil, P. and Bollinger, L., 2015. The aftershock sequence of the 2015 April 25  
476 Gorkha-Nepal earthquake, *Geophysical Journal International*, 203, 2119-2124, doi:  
477 10.1093/gji/ggv412.

478 Armijo, R., Tapponnier, P., Mercier, J.L. and Han, T.L, 1986. Quaternary extension in southern  
479 Tibet: Field observations and tectonic implications, *Journal of Geophysical Research: Solid*  
480 *Earth*, 91 (B14), 13803-13872.

481 Avouac, J.P., Meng, L., Wei, S., Wang, T. and Ampuero, J.P., 2015. Lower edge of locked Main  
482 Himalayan Thrust unzipped by the 2015 Gorkha earthquake, *Nature Geoscience*, 8, 708-711.

483 Bai, L., Liu, H., Ritsema, J., Mori, J., Zhang, T., Ishikawa, Y. and Li, G., 2015. Faulting structures  
484 above the Main Himalayan Thrust as shown by relocated aftershocks of the 2015 Mw7.8  
485 Gorkha, Nepal, earthquake, *Geophysical Research Letters*, 43, doi:10.1002/2015GL066473.

486 Baur, 2007. *Seismotectonics of the Himalayas and the Tibetan Plateau: Moment Tensor*  
487 *Analysis of Regional Seismograms*, Oregon State University, p.298.

488 Bettinelli, P., Avouac, J.P., Flouzat, M., Jouanne, F., Bollinger, L., Willis, P. and Chitrakar, G.R.,  
489 2006. Plate motion of India and interseismic strain in Nepal Himalaya from GPS and DORIS  
490 measurements, *Journal of Geodesy*, 80, 567-589, doi:10.1007/s00190-006-0030-3.

491 Bettinelli, P., Avouac, J.P., Flouzat, M., Bollinger, L., Ramillien G., Rajaure S. and Sapkota S.,  
492 2008. Seasonal variations of seismicity and geodetic strain in the Himalaya induced by  
493 surface hydrology, *Earth and Planetary Science Letters*, 266, 332-344,  
494 doi:10.1016/j.epsl.2007.11.02110.

495 Béjar-Pizarro, M., Carrizo, D., Socquet, A., Armijo, R., Barrientos, S., Bondoux, F., Bonvalot,  
496 S., Campos, J., Comte, D., de Chabalier, J.B., Charade, O., Delorme, A., Gabalda, G., Galetzka,  
497 J., Genricj, J., Nercessian, A., Olcay, M., Ortega, F., Ortega, I., Remy, O., Ruegg, J.C., Simons,  
498 M., Valderas, C. and Vigny, C., 2010. Asperities and barriers on the seismogenic zone in  
499 North Chile: state-of-the-art after the 2007 Mw 7.7 Tocopilla earthquake inferred by GPS  
500 and InSAR data, *Geophysical Journal International*, 183, 390-406, doi: 10.1111/j.1365-  
501 246X.2010.04748.x.

502 Bollinger, L., Avouac, J.P., Cattin, R. and Pandey, M.R., 2004a. Stress buildup in the Himalaya,  
503 *Journal of Geophysical Research*, 109, B11405, doi:10.1029/2003JB002911.

504 Bollinger, L., Avouac, J.P., Beyssac, O., Catlos, E.J., Harrison, T.M., Grove, M., Goffé, B. and  
505 Sapkota, S., 2004b. Thermal structure and exhumation history of the Lesser Himalaya in  
506 central Nepal, *Tectonics*, 23, TC5015, doi:10.1029/2003TC001564.

507 Bollinger, L., Perrier, F., Avouac, J.P., Sapkota, S., Gautam, U, and Tiwari, D.R., 2007.  
508 Seasonal modulation of seismicity in the Himalaya of Nepal, *Geophysical Research Letters*,  
509 34, L08304, doi:10.1029/2006GL029192.

510 Bollinger, L., Tapponnier, P., Sapkota, S.N. and Klinger, Y., 2016. Slip deficit in central Nepal:  
511 omen for a repeat of the 1344 AD earthquake?, *Earth, Planets and Space*, 68:12,  
512 doi:10.1186/s40623-016-0389-1.

513 Burtin, A., 2005. Seismotectonics of the Himalayan Arc from Regional Seismogram Moment  
514 Tensor Inversion, Internship report, Oregon State University.

515 Burtin, A., Bollinger, L., Vergne, J., Cattin R. and Nábělek J. L., 2008. Spectral analysis of  
516 seismic noise induced by rivers: A new tool to monitor spatiotemporal changes in stream  
517 hydrodynamics, *Journal of Geophysical Research*, 113, B05301, doi:10.1029/2007JB005034.

518 Cattin, R. and Avouac, J.P., 2000. Modeling mountain building and seismic cycle in the  
519 Himalaya of Nepal, *Journal of Geophysical Research*, 105(B6), 13389-13407.

520 Chanard, K., Avouac, J. P., Ramillien G. and Genrich J., 2014. Modeling deformation induced  
521 by seasonal variations of continental water in the Himalaya region: Sensitivity to Earth elastic  
522 structure, *Journal of Geophysical Research: Solid Earth*, 119, doi:10.1002/2013JB010451.

523 Collot, J. Y., Marcaillou, B., Sage, F., Michaud, F., Agudelo, W., Charvis, P., Graindorge, D.,  
524 Gutscher, M-A. and Spence, G., 2004. Are rupture zone limits of great subduction  
525 earthquakes controlled by upper plate structures? Evidence from multichannel seismic

526 reflection data acquired across the northern Ecuador–southwest Colombia margin, *Journal*  
527 *of Geophysical Research: Solid Earth*, 109, B11103.

528 Das, S. and Scholz, C.H., 1983. Why large earthquakes do not nucleate at shallow depths,  
529 *Nature*, 305, pp.621-623.

530 Dragert, H., Wang, K. and James, T. S., 2001. A silent slip event on the deeper Cascadia  
531 subduction interface, *Science*, 292(5521), 1525-1528.

532 Duputel, Z., Vergne, J., Rivera, L., Wittlinger, G., Farra, V. and Hetényi, G., 2016. The 2015  
533 Gorkha earthquake: A large event illuminating the Main Himalayan Thrust fault, *Geophysical*  
534 *Research Letters*, 43, doi: 10.1002/2016GL068083.

535 Elliott, J.R., Jolivet, R., Gonzalez, P.J., Avouac, J.P., Hollingsworth, J., Searle, M.P. and  
536 Stevens, V.L., 2016. Himalayan megathrust geometry and relation to topography revealed by  
537 Gorkha earthquake, *Nature geoscience*, 9, doi:10.1038/NGEO2623.

538 Fan, W. and Shearer P.M., 2015. Detailed rupture imaging of the 25 April 2015 Nepal  
539 earthquake using teleseismic P waves, *Geophysical Research Letters*, 42, 5744-5752, doi:  
540 10.1002/2015GL064587.

541 Grandin, R., Doin, M-P., Bollinger, L., Pinel-Puysegur, B., Ducret, G., Jolivet, R. and Sapkota,  
542 S.N., 2012. Long-term growth of the Himalaya inferred from interseismic InSAR  
543 measurement, *Geology*, 40, 12, 1059-1062, doi:10.1130/G33154.1.

544 Grandin, R., Vallée, M., Satriano, C., Lacassin, R., Klinger, Y., Simoes, M., and Bollinger, L.,  
545 2015. Rupture process of the Mw=7.9 2015 Gorkha earthquake (Nepal): insights into  
546 Himalayan megathrust segmentation, *Geophysical Research Letters*, 42, doi:  
547 10.1002/2015GL066044.

548 Haines, S.S., Klemperer, S.L., Brown, L., Jingru, G., Mechie, J., Meissner, R., Ross, A. and  
549 Wenjin, Z., 2003. INDEPTH III seismic data: From surface observations to deep crustal  
550 processes in Tibet, *Tectonics*, 22(8), 1001.

551 Huc, M., Hassani, R., and Chéry, J., 1998. Large earthquake nucleation associated with stress  
552 exchange between middle and upper crust, *Geophysical Research Letters*, 25 (4), 551-554.

553 Holtkamp, S. G. and Brudzinski, M. R., 2011. Earthquake swarms in circum-Pacific subduction  
554 zones, *Earth and Planetary Science Letters*, 305(1), 215-225.

555 Holtkamp, S. G., Pritchard, M. E. and Lohman, R. B., 2011. Earthquake swarms in south  
556 America, *Geophysical Journal International*, 187(1), 128-146.

557 Jackson, M., and Bilham, R., 1994. Constraints on Himalayan deformation inferred from  
558 vertical velocity fields in Nepal and Tibet, *Journal of Geophysical Research: Solid Earth*,  
559 99(B7), 13897-13912.

560 Jouanne, F., Mugnier, J.L., Gamond, J.F., Le Fort, P., Pandey, M.R., Bollinger, L., Flouzat, M.  
561 and Avouac, J.P., 2004. Current shortening across the Himalayas of Nepal, *Geophysical*  
562 *Journal International*, 157, 1-14, doi: 10.1111/j.1365-246X.2004.02180.x.

563 Khanal, S. and Robinson, D.M., 2013. Upper crustal shortening and forward modeling of the  
564 Himalayan thrust belt along the Budhi-Gandaki River, central Nepal, *International Journal of*  
565 *Earth Science (Geol Rundsch)*, 102, 1871-1891.

566 Kobayashi, T., Morishita, Y. and Yarai, H., 2015. Detailed crustal deformation and fault  
567 rupture of the 2015 Gorkha earthquake, Nepal, revealed from ScanSAR-based  
568 interferograms of ALOS-2, *Earth, Planets and Space*, 67, 201, doi: 10.1186/s40623-015-0359-  
569 z.

570 Kumahara, Y., Chamlagain, D., Upreti, B. N., 2016. Geomorphic features of active faults  
571 around the Kathmandu Valley, Nepal, and no evidence of surface rupture associated with  
572 the 2015 Gorkha earthquake along the faults, *Earth, Planets and Space*, 68(1), 1-8.

573 Métois, M., Socquet, A. and Vigny, C., 2012. Interseismic coupling, segmentation and  
574 mechanical behavior of the central Chile subduction zone, *Journal of Geophysical Research*,  
575 117, B03406, doi:10.1029/2011JB00736.

576 Murphy, M. A., Taylor, M. H., Gosse, J., Silver, C. R. P., Whipp, D. M. and Beaumont, C., 2014.  
577 Limit of strain partitioning in the Himalaya marked by large earthquakes in western Nepal,  
578 *Nature Geoscience*, 7(1), 38-42.

579 Nábelek, J., 1984. Determination of earthquake source parameters from inversion of body  
580 waves. Ph. D. thesis, Massachusetts Institute of Technology, Cambridge, MA.

581 Nábelek, J. and Xia, G., 1995. Moment-tensor analysis using regional data: Application to the  
582 25 March, 1993, Scotts Mills, Oregon, earthquake, *Geophysical Research Letters*, 22(1), 13–  
583 16.

584 Nabelek, J., Hetényi, G., Vergne, J., Sapkota, S.N., Kafle, B., Jiang, M., Su, H., Chen, J., Huang,  
585 B-S. and Hi-CLIMB team, 2009. Underplating in the Himalaya-Tibet Collision Zone Revealed  
586 by the Hi-CLIMB Experiment, *Science*, 325, 1371-1374.

587 Nakata, T., 1989. Active faults of the Himalaya of India and Nepal, *Geological Society of*  
588 *America Special Papers*, 232, 243-264.

589 Pandey, M.R., 1985. Seismic model of central and eastern lesser Himalaya of Nepal, *Journal*  
590 *of Nepal Geological Society*, 3(1-2), 1-11.

591 Pandey, M.R., Tandukar, R.P., Avouac, J.P., Lavé, J. and Massot, J.P., 1995. Interseismic strain  
592 accumulation on the Himalayan Crustal Ramp (Nepal), *Geophysical Research Letters*, 22,  
593 751-754.

594 Pandey, M.R., Tandukar, R.P., Avouac, J.P., Vergne, J. and Héritier, T., 1999. Seismotectonics  
595 of the Nepal Himalayas from a local seismic network, *Journal of Asian Earth Sciences.*, 17(5-  
596 6), 703-712.

597 Pearson, O.N. and DeCelles, P.G., 2005. Structural geology and regional tectonic significance  
598 of the Ramgarh thrust, Himalayan fold-thrust belt of Nepal, *Tectonics*, 24, TC4008, doi:  
599 10/1029/2003TC001617.

600 Robinson, D.M., DeCelles, P.G., Patchett, P.J. and Garzione, C.N, 2001. The kinematic  
601 evolution of the Nepalese Himalaya interpreted from Nd isotopes, *Earth and Planetary  
602 Science Letters*, 192, 4, 507-521, doi:10.1016/S0012-821X(01)00451-4.

603 Sapkota S.N. ,2011. Surface rupture of 1934 Bihar-Nepal earthquake: implications for seismic  
604 hazard in Nepal Himalaya, Ph.D thesis, Institut de Physique du Globe de Paris,France. pp 2-  
605 292.

606 Saul, J., Kumar, M.R. and Sarkar D., 2000. Lithospheric and upper mantle structure of the  
607 Indian shield, from receiver functions, *Geophysical Research Letters*, 27, 2357–2360.

608 Schmidt, D. A. and Gao, H., 2010. Source parameters and time-dependent slip distributions  
609 of slow slip events on the Cascadia subduction zone from 1998 to 2008, *Journal of  
610 Geophysical Research: Solid Earth*, 115, B00A18, doi:10.1029/2008JB006045.

611 Schulte-Pelkum, V., Monsalve, G., Sheehan, A., Pandey, M.R., Sapkota, S., Bilham, R. and Wu,  
612 F., 2005. Imaging the Indian subcontinent beneath the Himalaya, *Nature Letters*, 435,  
613 doi:10.1038/nature03678.

614 Schwartz, S. Y., Dewey, J. W. and Lay, T. 1989. Influence of fault plane heterogeneity on the  
615 seismic behavior in the southern Kurile Islands Arc, *Journal of Geophysical Research: Solid*  
616 *Earth*, 94(B5), 5637-5649.

617 Schwartz, S. Y. and Rokosky, J. M., 2007. Slow slip events and seismic tremor at  
618 circum-Pacific subduction zones, *Reviews of Geophysics*, 45(3).

619 Shrestha, A.B., Wake, C.P., Dibb, J.E, Mayewski, P.A., 2000. Precipitation fluctuations in  
620 Nepal Himalaya and its vicinity and relationship with some large scale climatological  
621 parameters, *International Journal of Climatology*, 20, 317 – 327.

622 Souloumiac, P., Leroy, Y.M., Maillot, B. and Krabbenhoft, K., 2009. Predicting stress  
623 distributions in fold-and-thrust belts and accretionary wedges by optimization, *Journal of*  
624 *Geophysical Research*, 114, B09404, doi: 10.1029/2008JB005986.

625 Stevens, V.L. and J.P. Avouac, 2015. Interseismic coupling on the main Himalayan thrust,  
626 *Geophysical Research Letters*, 42, 5828–5837, doi:10.1002/2015GL064845.

627 Szeliga, W., Melbourne, T., Santillan, M. and Miller, M., 2008. GPS constraints on 34 slow slip  
628 events within the Cascadia subduction zone, 1997–2005, *Journal of Geophysical Research:*  
629 *Geophysical Research*, v.110, *Solid Earth*, 113, B04404, doi:10.1029/2007JB004948.

630 Waldhauser, F. and Ellsworth, W.L., 2000. A double-difference earthquake location  
631 algorithm: method and application to the Northern Hayward Fault, California, Bulletin  
632 Seismological Society of America, 90 (6), 1353-1368.

633 Yatagai, A., Kamiguchi, K., Arakawa, O., Hamada, A., Yasutomi, N. and Kitoh, A., 2012.  
634 Aphrodite. Constructing a long-term daily gridded precipitation dataset for Asia based on a  
635 dense network of rain gauges, America Meteorological Society, Q07023, doi:  
636 10.1029/2011GC003513.

637 Zahradnik, J., Jansky, J. and Plicka, V., 2008. Detailed waveform inversion for Moment Tensor  
638 of  $M \sim 4$  events: examples from Corinth Gulf, Greece, Bulletin of the Seismological Society of  
639 America, 98 (6), pp. 2756-2771, doi: 10.1785/0120080124.

#### 640 **Table caption**

641 Table 1. Description of the main shocks of the three swarms of 1997. Origin time and  
642 epicentral location are from the NSC.

#### 643 **Figure captions**

644 Figure 1. Seismicity map of Central Nepal from the National Seismological Center of Nepal  
645 (Modified from Adhikari et al., 2015). Red dots are the aftershocks of the Gorkha earthquake  
646 and the yellow dots indicate epicenters prior to the Gorkha event since 1994. The iso-slip  
647 contours of the Gorkha earthquake are from Grandin et al., 2015. The black rectangle  
648 indicates the area used for Figure 2 and 4. Past earthquakes rupture areas (top right) from  
649 Bollinger et al., 2016. MFT: Main Frontal Thrust, MBT: Main Boundary Thrust, MCT: Main  
650 Central Thrust. The orange thin lines are the traces of the Southern Tibetan Grabens (Armijo  
651 et al., 1986)

652 Figure 2. Cumulative number of events during the interseismic period recorded by the NSC  
653 from 1994 to 2015 in the area delimited in Figure 1. The black line corresponds to the events  
654 of magnitude  $ML \geq 2.0$  scaled on the left side. The gray diamonds correspond to the events of  
655 magnitude  $ML \geq 4.0$  scaled on the right side. 30% of the events of  $ML \geq 4.0$  occurred in 1997.

656 Figure 3. Centroid Moment Tensor solution for the Sarshin earthquake occurred on January  
657 31<sup>st</sup> 1997. For each station, observations are shown with solid lines and synthetics with  
658 dotted lines. Z, R and T are the vertical, radial and transverse components respectively.  
659 Radial components of CHTO, HYB and WUS were discarded because of the high signal-noise  
660 ratio. 1 and 0 are the weights used in the inversion.

661 Figure 4. Spatial distribution of the seismic episode of 1996-1999, north of Kathmandu (see  
662 Figure 1): The map shows the relocated seismicity as a function of time and magnitude of  
663 Zone 1 and 2 (zones boundary: longitude  $85.4^\circ$ ). The main shock corresponds to the 1997  
664 January 31<sup>st</sup>  $ML=5.8$  ( $M_w 4.8$ ) earthquake with the preferred focal mechanism plane in red.  
665 The cross-sections include the relocated seismicity. A-A' and B'-B cross-sections are  
666 orientated N140 and N065, respectively. They stack seismicity located 10 km for A-A' and 3  
667 km for B'-B from each side of the track. The area highlighted in light white correspond to the  
668 suspected fault segments at depth activated by the 1997 episode (see Figure 7 for  
669 interpretation). The intersection between A-A' and B-B' cross-sections are indicated with a  
670 black cross. The green, blue and pink-brown lines at the bottom of the map are western,  
671 central and eastern respectively used in Figure 5.

672 Figure 5. Time sequence of the seismicity north of Kathmandu. The zones are indicated at  
673 the bottom of the map in Figure 4. The Sarshin earthquake is indicated by the yellow star.  
674 The red dashed line is the average rate of seismicity (108 events per year).

675 Figure 6. Spatio-temporal variations of the seismicity. A) Normalized time sequence of the  
676 midcrustal seismicity along the MHT. The curves correspond to the three swarm areas and  
677 the yellow one to the inter-swarms area. Gray shadow zone is the time covered in the map.  
678 B) Midcrustal seismicity for the period 1996-1997 in yellow, swarm seismicity in red.  
679 Orange circles are the Southern Tibetan Grabens north of the swarms.

680 Figure 7. Schematic evolution of the stress field and structure activation. A) Variation of  
681 shear stress and normal stress associated with a transient slip event on the Main Himalayan  
682 Thrust in a region with midcrustal tear faults and southern Tibetan grabens. The initial state  
683 is shown in black and is assumed tangent to the failure envelope represented by the straight  
684 line. 1, 2, and 3 refer to the different areas indicated in B and C. In area 1,  $s_1$  and  $s_3$  are  
685 horizontal, increasing and decreasing respectively, promoting failure. In area 2,  $s_1$  is  
686 horizontal, striking about north-south and increasing during interseismic deformation and  
687 transient slip events, promoting failure. In area 3,  $s_3$  is horizontal, striking approximately  
688 east-west and decreasing during interseismic deformation, promoting failure. B) and C)  
689 Kinematical evolution north of Kathmandu in 1996-1997; orange surface corresponds to the  
690 area with a coupling >50-80% depending on source (Ader et al., 2012; Grandin et al., 2015).  
691 B) Static stress change induced by slip on the tear fault is schematized by Coulomb stress  
692 lobes, respectively blue and red for  $DCFF < 0$  and  $> 0$ . Dotted lines and filled areas correspond  
693 respectively to the  $DCFF$  calculated for receiver faults with the backthrust and the thrust  
694 orientation (more information in Table S1, Table S2, and Figure S8 to S11). C) Activation of  
695 the backthrust (in green) and the thrust fault (in salmon) as a consequence of static stress  
696 change induced by the tear fault (B). D) Schematic three dimensional block, with vertical  
697 exaggeration, of the MHT with the backthrust (green) and the tear fault (purple). Colors on  
698 the MHT correspond to the coupling: red: total coupling (>50-80%), orange: transition zone

699 (60%-40%), Yellow: completely decoupled (0%) (Ader et al., 2012; Grandin et al., 2015).

700 White arrows show the kinematics of the structures.

701

702

703

Table

[Click here to download Table: Table1.docx](#)

Main shocks of swarms	Date	Time	Longitude	Latitude	Depth (km)	Magnitude			Focal Mechanism					
						ML (a)	mb (b)	Mw (c)	NP1			NP2		
									Strike (°)	Dip (°)	Rake (°)	Strike (°)	Dip (°)	Rake (°)
Sarshin	31/01/1997	20 :02 :14	85.34°E	28.04°N	20.3(a), 7.0 (fixed)(b), 17(c), 23(d), 22.2(e), 21(f), 17.6(g)	5.8	5.2	4.8 (c)	74.6 (c)	84.8	66.4	332.2	24.1	67.1
Darchula	05/01/1997	08 :47 :24	80.42°E	29.90°N	13 24.9 15(h)	6.3	5.4	5.4 (e) 5.5 (h)	279 (h)	19	68	122	73	97
Gudelhongu	30/12/1996	11 :18 :19	86.91°E	27.22°N	25 33 (f)	5.8	4.8	-						

- (a) National Seismological Center of Nepal (NSC).
- (b) International Seismological Centre, UK (ISC)
- (c) Centroid Moment Tensor (in this article)
- (d) Geophysical Survey of Russian Academy of Science (MOS)
- (e) National Earthquake Information Center, USGS (NEIC)
- (f) Experimental (GSETT3) International Data Center, USA (EIDC)
- (g) Engdahl, van der Hilst and Buland, USA (EHB)
- (h) Global Centroid Moment Tensor

Figure (figure caption in manuscript\_revised)

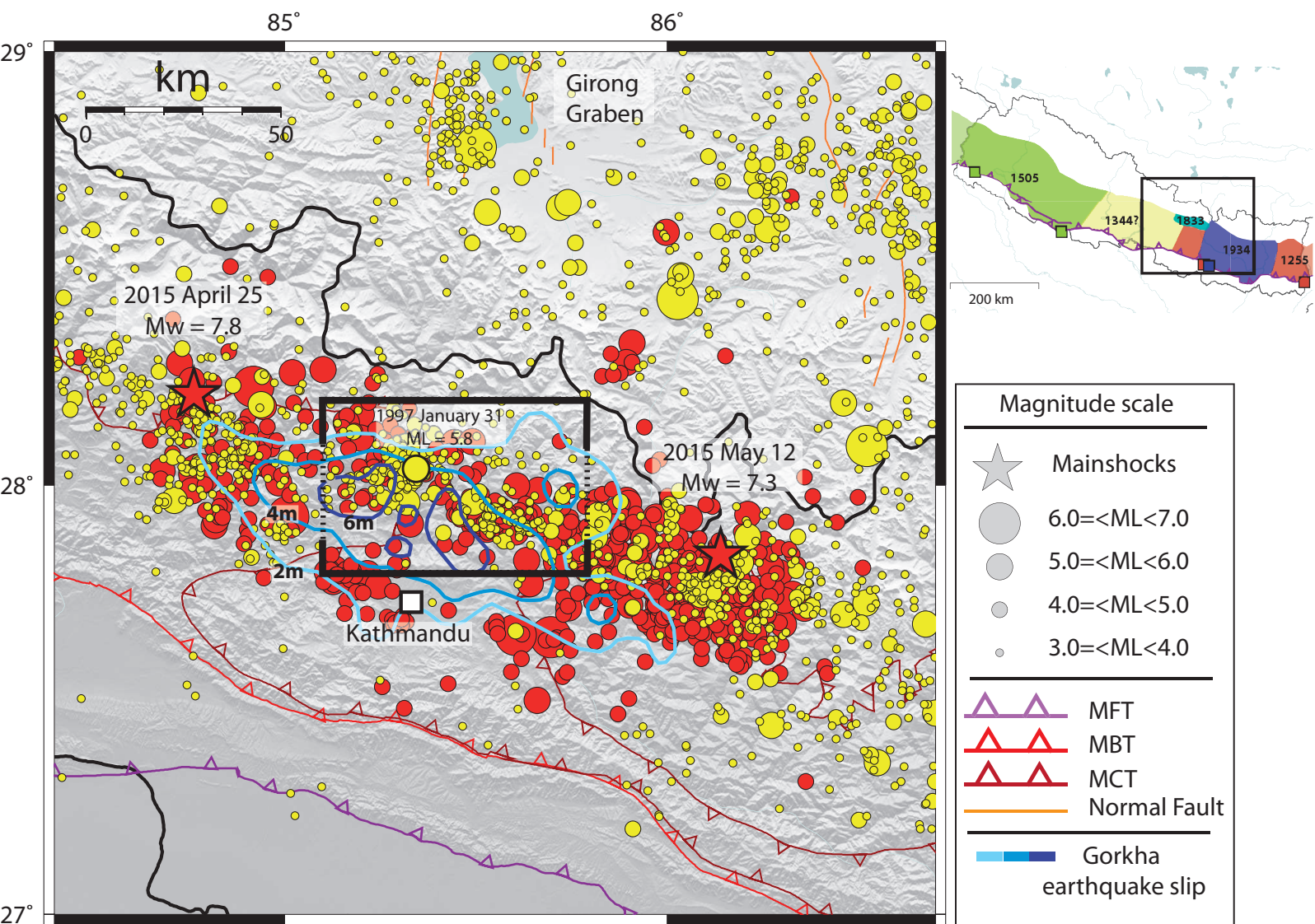
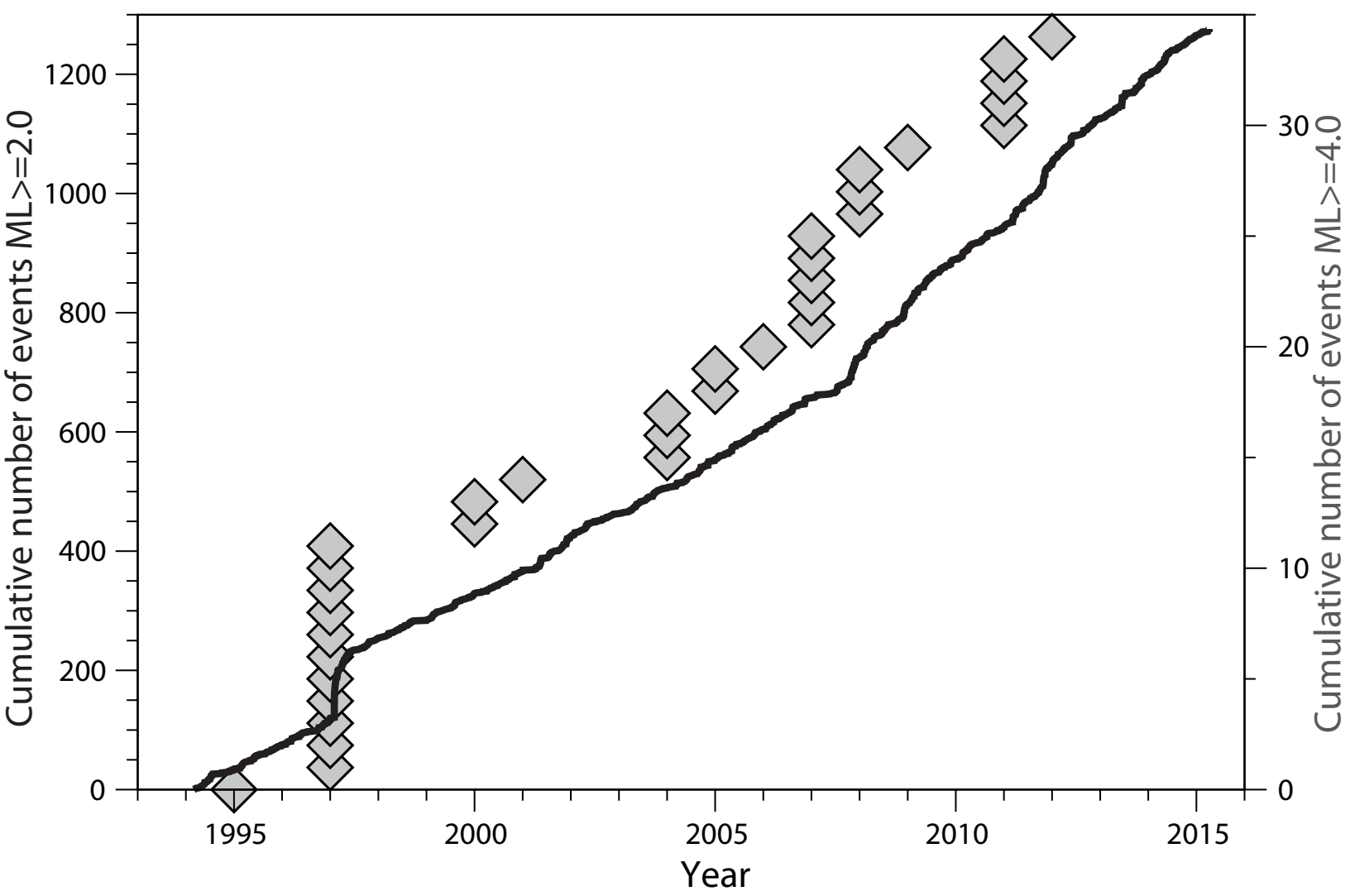
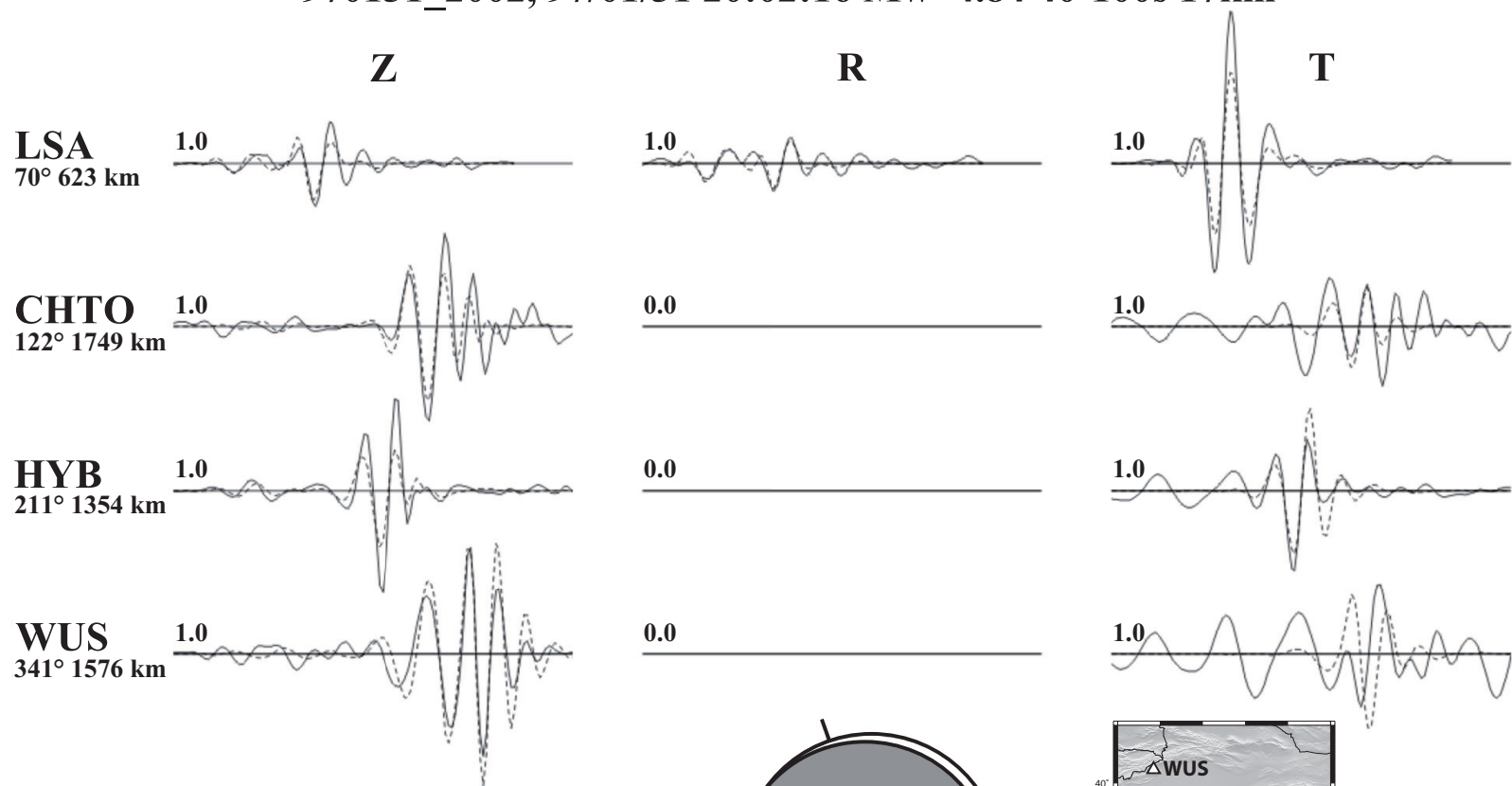


Figure (figure caption in manuscript\_revised)



970131\_2002, 97/01/31 20:02:16 Mw=4.84 40-100s 17km



0 100 200 300 400 500

Time (s)

maximum amplitude: 2.7 μm

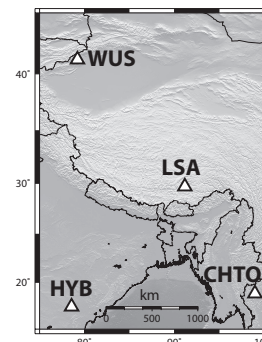


Figure (with caption below and on the same page)

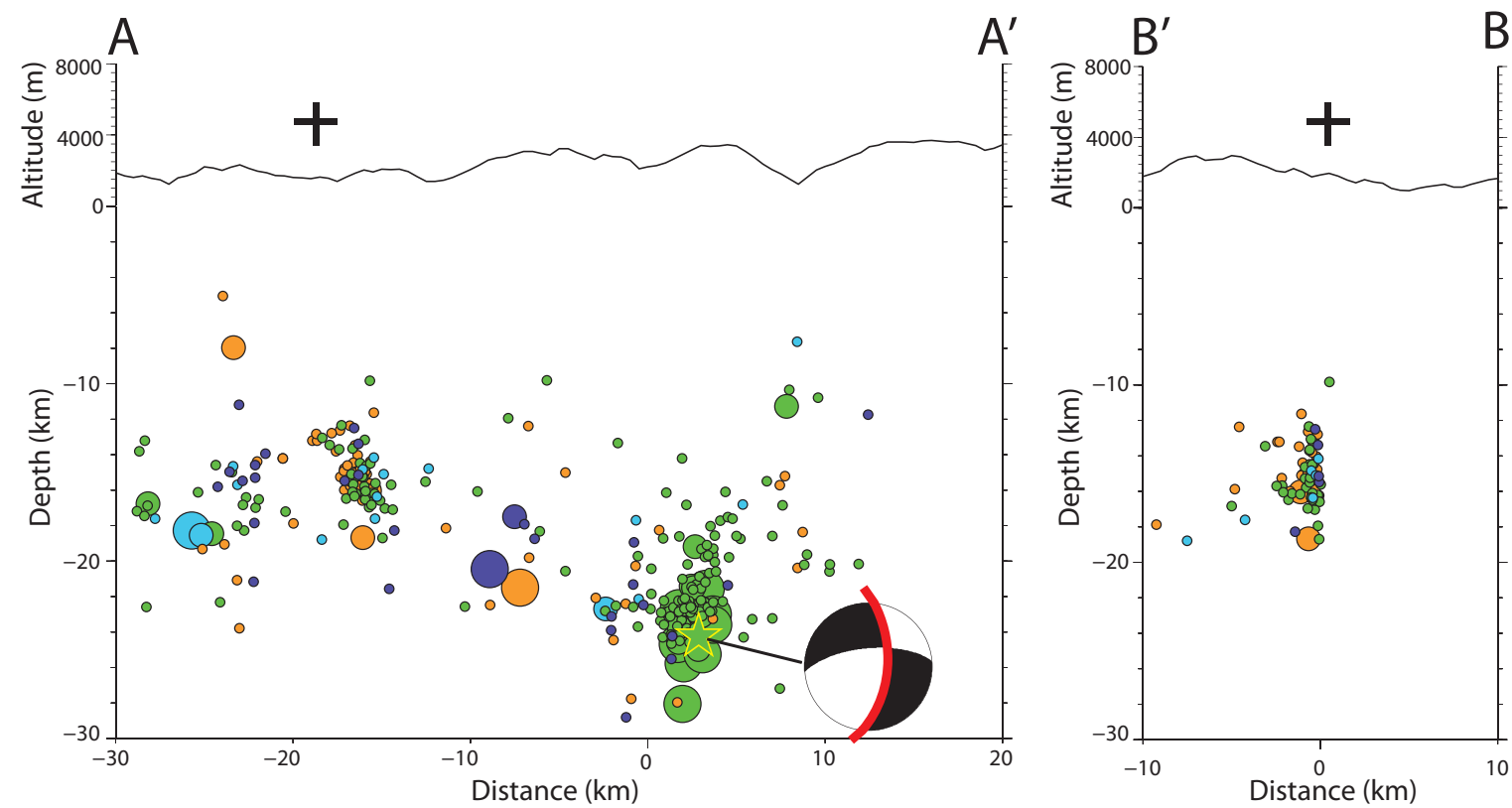
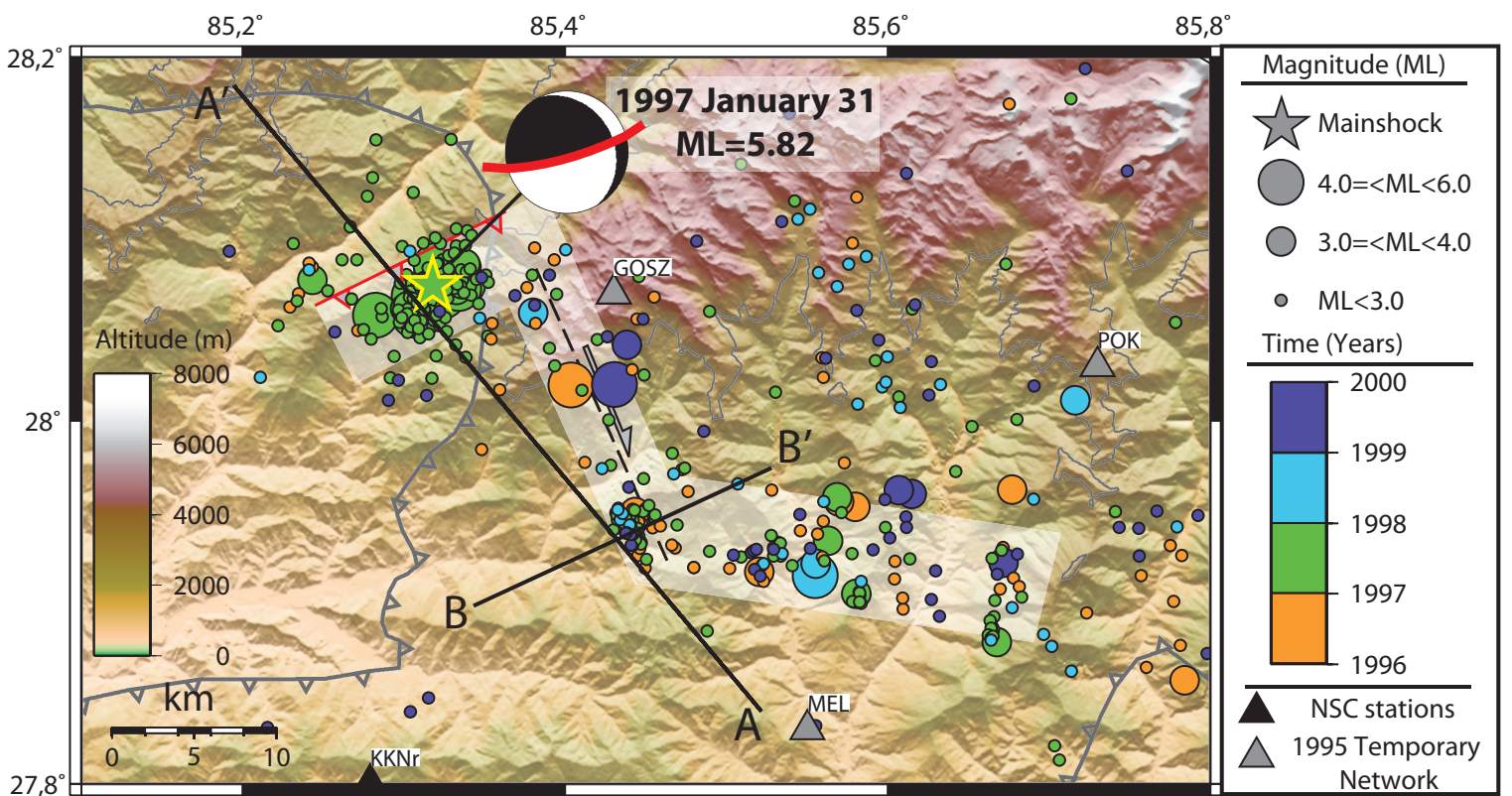
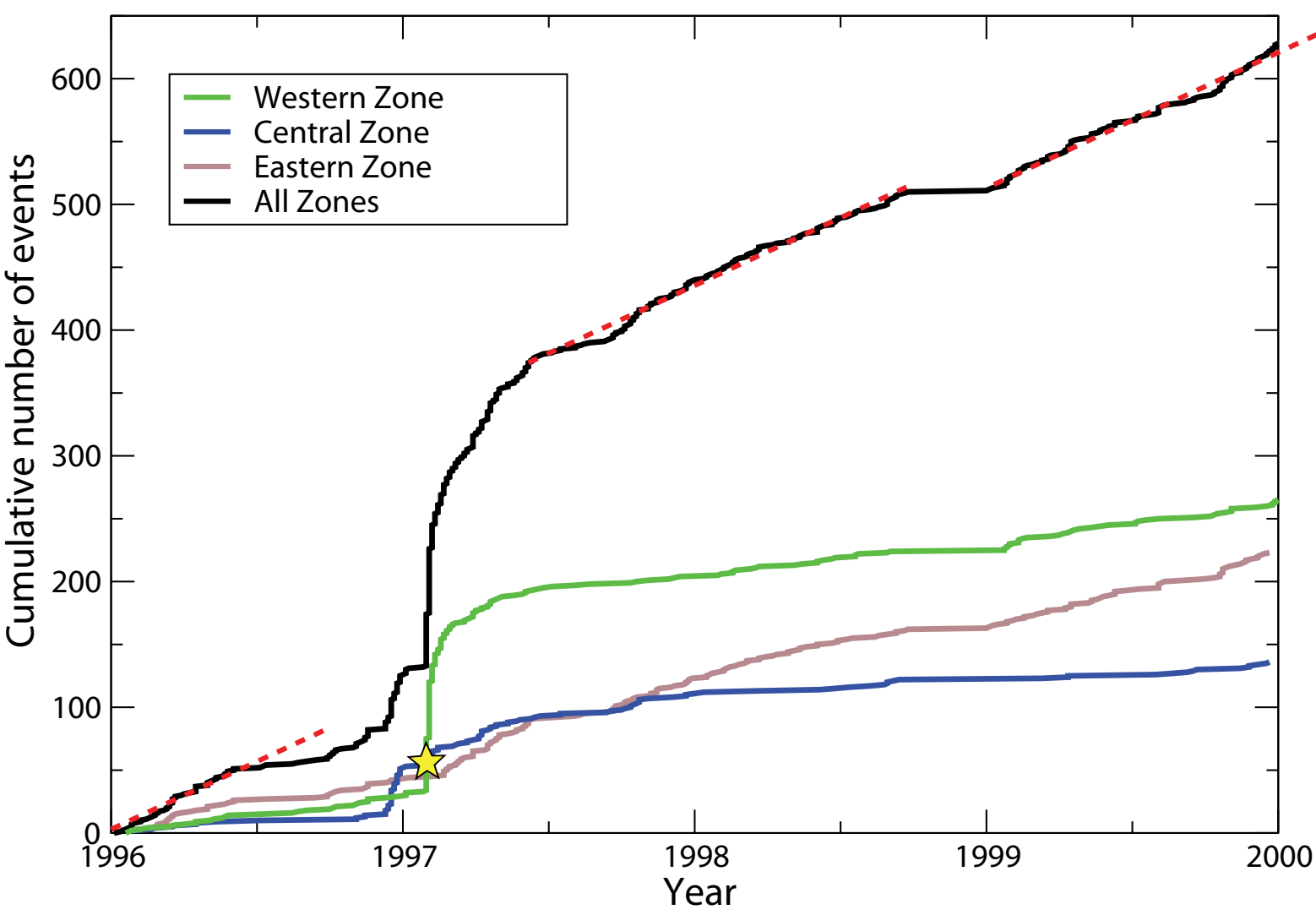


Figure (with caption below and on the same page)



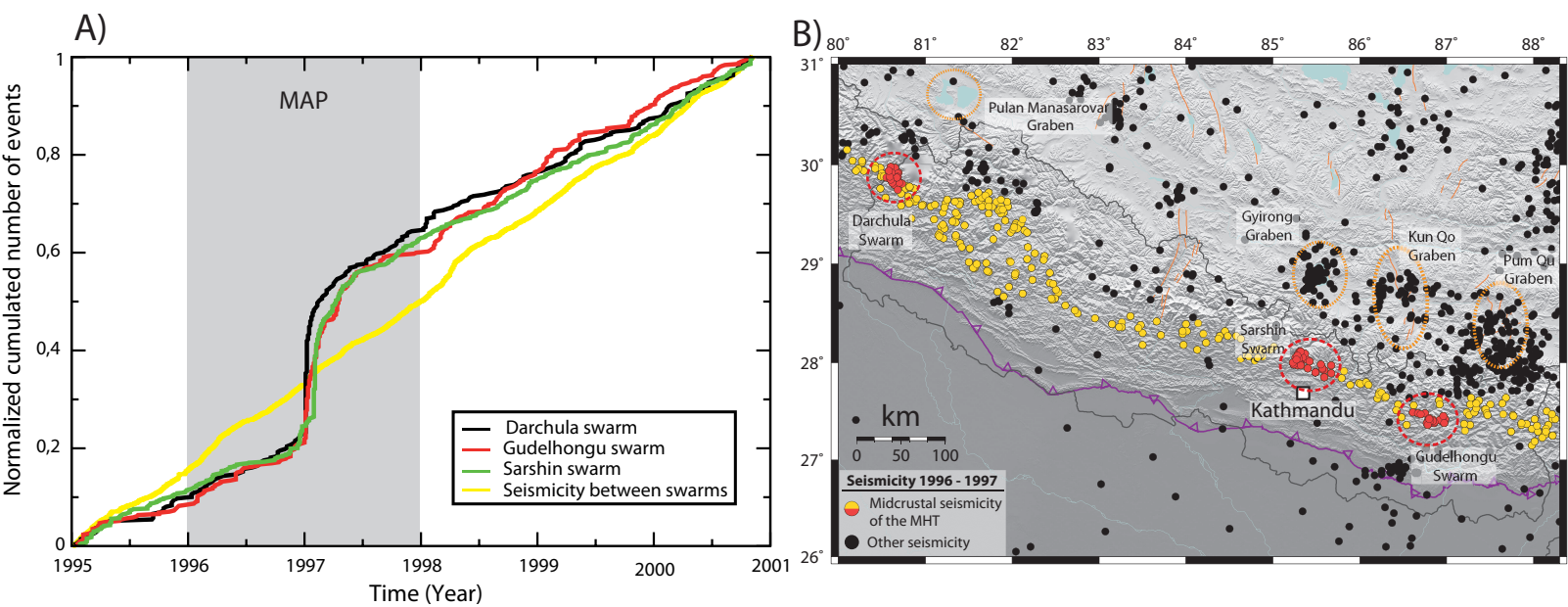
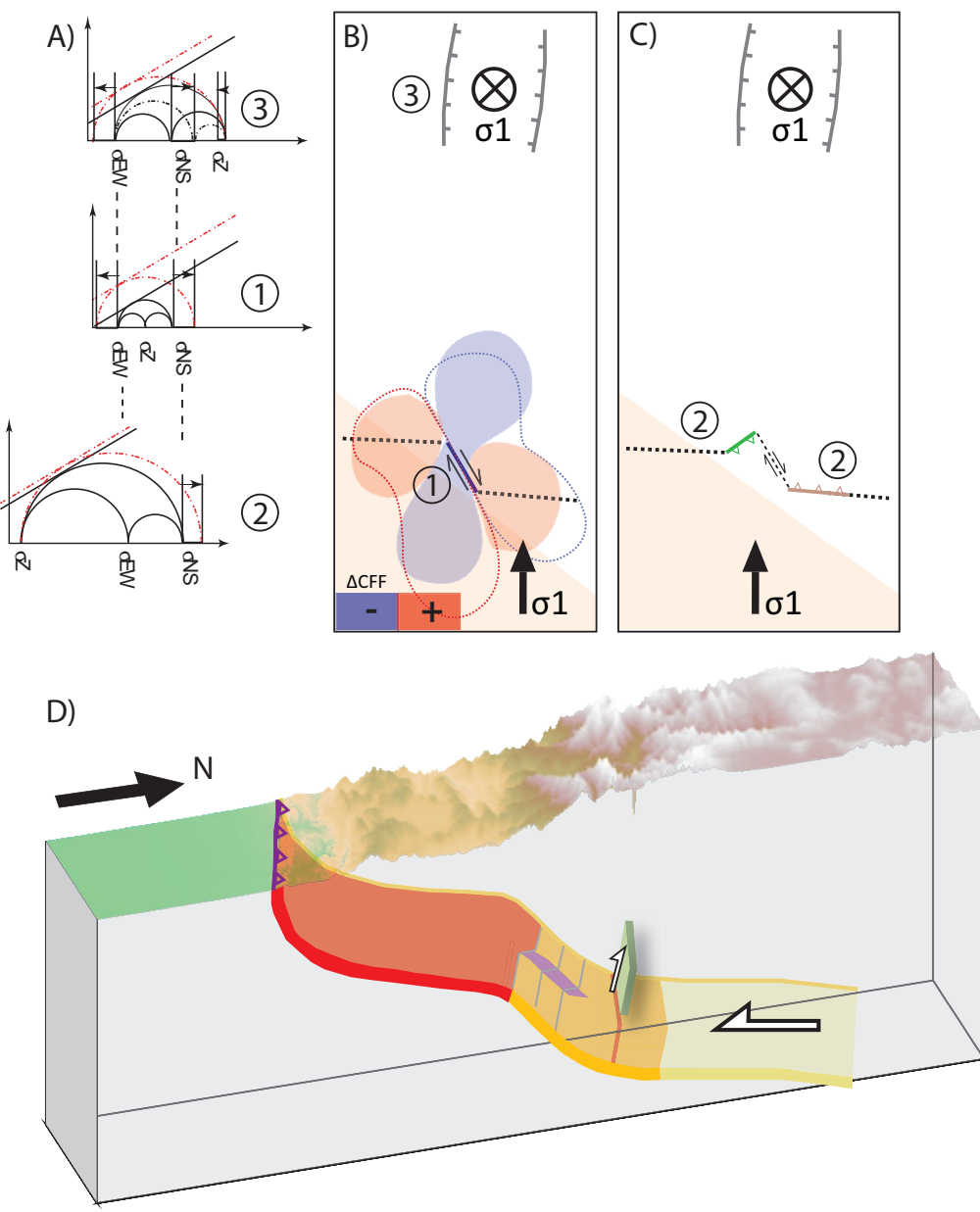


Figure (figure caption in manuscript\_revised)



**Supplementary material for online publication only**

**[Click here to download Supplementary material for online publication only: SupplMaterial.pdf](#)**